

Lawrence Berkeley National Laboratory

LBL Publications

Title

Double-Helical Tiled Chain Structure of the Twist-Bend Liquid Crystal Phase in CB7CB

Permalink

<https://escholarship.org/uc/item/5rf2q38s>

Journal

Crystals, 14(7)

ISSN

2073-4352

Authors

Tuchband, Michael R

Shuai, Min

Graber, Keri A

et al.

Publication Date

2024-07-01

DOI

10.3390/cryst14070583






Copyright Information

This work is made available under the terms of a Creative Commons Attribution License, available at <https://creativecommons.org/licenses/by/4.0/>

Peer reviewed

Article

Double-Helical Tiled Chain Structure of the Twist-Bend Liquid Crystal Phase in CB7CB

Michael R. Tuchband ^{1,2,†}, Min Shuai ^{1,2,†}, Keri A. Graber ^{1,2}, Dong Chen ^{1,2}, Chenhui Zhu ³, Leo Radzihovsky ^{1,2}, Arthur Klitnick ^{1,2}, Lee Foley ^{2,4}, Alyssa Scarbrough ^{2,4}, Jan H. Porada ^{2,4}, Mark Moran ^{2,4}, Joseph Yelk ^{1,2}, Justin B. Hooper ^{2,5}, Xiaoyu Wei ^{2,5} , Dmitry Bedrov ^{2,5}, Cheng Wang ³, Eva Korblova ^{2,4} , David M. Walba ^{2,4} , Alexander Hexemer ³, Joseph E. Maclennan ^{1,2} , Matthew A. Glaser ^{1,2}  and Noel A. Clark ^{1,2,*}

¹ Department of Physics, University of Colorado, Boulder, CO 80309, USA

² Soft Materials Research Center, University of Colorado, Boulder, CO 80309, USA

³ Advanced Light Source, Lawrence Berkeley National Laboratory, Berkeley, CA 94720, USA

⁴ Department of Chemistry and Biochemistry, University of Colorado, Boulder, CO 80309, USA

⁵ Department of Materials Science and Engineering, The University of Utah, Salt Lake City, UT 84112, USA

* Correspondence: noel.clark@colorado.edu

† These authors contributed equally to this work.

Abstract: The twist-bend nematic liquid crystal phase is a three-dimensional fluid in which achiral bent molecules spontaneously form an orientationally ordered, macroscopically chiral, heliconical winding of a ten nanometer-scale pitch in the absence of positional ordering. Here, the structure of the twist-bend phase of the bent dimer CB7CB and its mixtures with 5CB is characterized, revealing a hidden invariance of the self-assembly of the twist-bend structure of CB7CB, such that over a wide range of concentrations and temperatures, the helix pitch and cone angle change as if the ground state for a pitch of the TB helix is an inextensible heliconical ribbon along the contour formed by following the local molecular long axis (the director). Remarkably, the distance along the length for a single turn of this helix is given by $2\pi R_{\text{mol}}$, where R_{mol} is the radius of bend curvature of a single all-trans CB7CB molecule. This relationship emerges from frustrated steric packing due to the bent molecular shape: space in the fluid that is hard to fill attracts the most flexible molecular subcomponents, a theme of nanosegregation that generates self-assembled, oligomer-like correlations of interlocking bent molecules in the form of a brickwork-like tiling of pairs of molecular strands into duplex double-helical chains. At higher temperatures in the twist-bend phase, the cone angle is small, the director contour is nearly along the helix axis z , and the duplex chains are sequences of biaxial elements formed by overlapping half-molecule pairs, with an approximately 45° rotation of the biaxis between each such element along the chain.

Keywords: liquid crystals; twist-bend; heliconical; dimers; RSoXS



Citation: Tuchband, M.R.; Shuai, M.; Graber, K.A.; Chen, D.; Zhu, C.; Radzihovsky, L.; Klitnick, A.; Foley, L.; Scarbrough, A.; Porada, J.H.; et al. Double-Helical Tiled Chain Structure of the Twist-Bend Liquid Crystal Phase in CB7CB. *Crystals* **2024**, *14*, 583. <https://doi.org/10.3390/cryst14070583>

Academic Editor: Francesco Simoni

Received: 11 May 2024

Revised: 20 June 2024

Accepted: 21 June 2024

Published: 25 June 2024



Copyright: © 2024 by the authors. Licensee MDPI, Basel, Switzerland. This article is an open access article distributed under the terms and conditions of the Creative Commons Attribution (CC BY) license (<https://creativecommons.org/licenses/by/4.0/>).

1. Introduction

An important theme in soft materials and liquid crystal (LC) science is to understand the interplay between molecular shape and macroscopic self-organization and create new motifs of ordering based on the exploration of different molecular shapes. A prime example of such a scenario has been the discovery of the spontaneous formation of chiral ordering in fluids (Pasteur's experiment in fluids), as evidenced by macroscopic chiral conglomerate domains in liquid crystals of achiral bent molecules [1,2]. In these fluid lamellar phases, the confinement of the molecules to layers forces their steric bend to be in a common, in-layer direction, giving long-ranged polar ordering, and the steric ordering of molecular tilt direction gives macroscopic chirality [3,4]. Diverse motifs of frustrated packing of

achiral molecules in these materials lead to chiral isotropic liquids [5], chiral fluid three-dimensional (3D) crystals [6], columnar phases [7,8], helical nanofilament phases [9], and chiral sponge phases [10].

The most recent, and perhaps most exotic, manifestation of spontaneous chirality in a fluid of achiral molecules is the twist-bend (TB) liquid crystal phase formed of bent molecular dimers, like CB7CB (Figure 1a), which fills 3D space with a long-range ordered, 1D helical precession of pure molecular orientation, sketched in Figure 1b–e. Initially proposed as a theoretical possibility [11–13], the TB phase has been realized [14,15] and intensively studied in a number of systems of bent molecules [15–25]. This activity has featured TB applications development, including fast electro-optic switching in the TB phase [26] and pretransitional TB clustering, enabling the spectacular tunability of the helical nematic helix in TB systems with chiral doping, a significant advance over existing chiral nematic technologies [27,28].

This spontaneously chiral structure is nematic with infinite helical symmetry: there is no coherent modulation of the density accompanying the helix, as evidenced by the absence of non-resonant X-ray diffraction sensitive to positional ordering [15,29], whereas resonant X-ray diffraction, which probes molecular orientation, reveals the helical periodicity [30,31]. A remarkable feature of this phase is its very short pitch, on the order of four molecular lengths in CB7CB, as illustrated in Figure 1d. In typical nematic LC phases, even strongly chiral ones, neighboring molecules differ in their long-axis orientation by only a few degrees at most. Phases with larger orientational jumps are always accompanied by positional ordering into 1D lamellar, 2D columnar, or 3D crystalline phases. How the TB phase remains a fully 3D liquid in the presence of such strong, coherent internal orientational ordering is the key question addressed here.

In this paper, we probe the structure of the TB phase and develop a new model for its nanoscale organization. To explore the nanoscale structure of the TB phase, we have carried out resonant and non-resonant soft X-ray scattering (RSoXS) and birefringence experiments, measuring the helix pitch and cone angle in a series of CB7CB mixtures with nematic liquid crystal 5CB, and determining the ground state helix structures of TB phases. Of particular interest here is the question, “Is the N_{TB} phase compatible with a continuum description despite its very short pitch? [32]”, which has been extensively debated in the literature [33–35].

In the conventional nematic (N) liquid crystal phase, the ground state is a three-dimensional (3D) fluid of uniform density with an orientation field of molecular rods in which the local average molecular long axis, the director field, $\mathbf{n}(\mathbf{r})$, has uniform orientation in space [36]. The twist-bend nematic LC phase is also a 3D fluid of uniform density but composed of bent molecules that self-assemble into a chiral helical ground state, with a helical precession of $\mathbf{n}(\mathbf{z})$ in azimuthal orientation $\varphi(\mathbf{z})$ on a cone of angle θ_H ; the helix (H) is coaxial with an axis z and has a pitch of ~ 10 -nanometer scale (Figure 1c–e) [29,30,37]. This chiral structure forms by a symmetry-breaking transition from the uniaxial nematic, even though the molecules are structurally achiral. The resulting helical director field has bend and twist elastic deformations of $\mathbf{n}(\mathbf{z})$ that are nonzero and of uniform magnitude, B_H and T_H , respectively, everywhere in space (Figure 1c–f, [12]). Recently, resonant soft X-ray scattering (RSoXS), by virtue of its sensitivity to molecular orientation, has enabled observation of scattering from this TB helix in the bent molecular dimer CB7CB, where the magnitude of the wavevector of the diffraction peak, $|q| = q_H$, is a direct measure of the pitch of the TB helix along z , $p_H = 2\pi/q_H$ [30,31], with the pitch in the $p_H \sim 10$ nm range, a few molecular lengths. These data are somewhat surprising in that p_H does not increase substantially as $\theta_H \rightarrow 0$ on approaching the transition to the N phase.

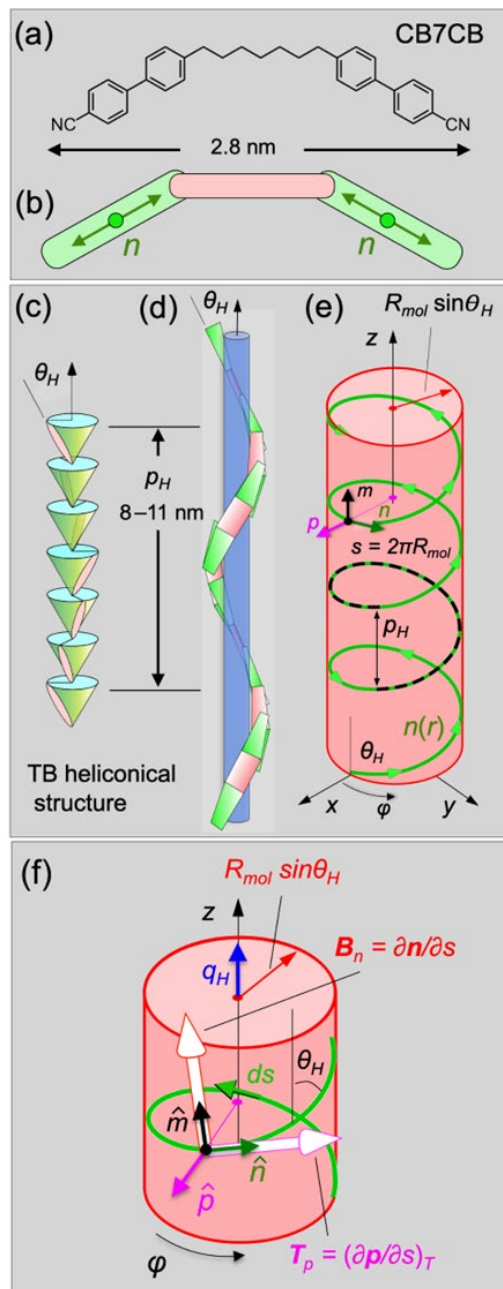


Figure 1. (a) CB7CB, the bent molecular dimer studied. (b) Bent-rod representation of CB7CB, showing its two contributions to the director field, the unit vector $n(r)$. Schematic structures of the twist-bend nematic (TB) phase, showing (c) the precession of the director orientation on a cone of angle θ_H , taken for here to be the tilt of a principal axis of the dielectric tensor. (d) Helical winding of the director in the TB phase. At each level, the indicated orientations fill the x - y plane. (e) Geometry of the helical path of the contour line that locally follows the orientation of $n(r)$. The distance along the contour is $s(\varphi)$. A physical constraint of the TB structure in CB7CB, first reported in this paper, is that the cylinder radius varies with cone angle θ_H as $\sin\theta_H$, such that the length of the contour $s(2\pi)$ for one pitch of the helix (dashed black line) is independent of θ_H and always given by $s(2\pi) = 2\pi R_{mol}$, where R_{mol} is the bend radius of curvature of an extended CB7CB molecule. (f) Geometry of reorientation on the director contour line as defined by the vectors of reorientation. Of relevance to the TB phase is $B_n(r)$, the bend rotation of $n(r)$ about auxiliary vector $m(r)$, and $T_p(r)$, the twist rotation of the biaxial vector $p(r)$ about $n(r)$. The magnitudes of these deformations, B_H and T_H are uniform in space and, under the constraint noted above, satisfy the condition $B_H^2 + T_H^2 = 1/R_{mol}^2$, describing the exchange of director bend for biaxial twist as θ_H is decreased.

Combination of q_H data with measurements of the average helical cone angle θ_H suffices to determine the essential mean geometry of the TB helix as temperature and mixture concentration of 5CB are changed, including calculation of the magnitude of the local director bend B_H and its dependence on cone angle θ_H , as discussed in a preliminary version of this work [38] and its review [39]. This analysis produces unexpected, remarkable results: (i) the only molecular parameter governing the relation between B_H and θ_H is B_{mol} , the nanometer-scale bend curvature radius of a single CB7CB molecule; (ii) the TB structure features a hidden self-generated internal constraint, wherein s , the length of a period of the helix along the contour line following the local molecular long axis (the director), is an invariant, $s \approx 2\pi/B_{mol}$, independent of θ_H , i.e., nearly the same for all concentrations and temperatures; (iii) such a constraint can only arise from longitudinal nanoscale structuring along the director contour that is not encoded in the geometry of $n(z)$. What we find is steric oligomerization: transient association of molecules into linear oligomer-like chains that combine to form a duplex helical, brickwork-like tiled chain; (iv) these duplex chains behave in turn as helical steric objects which pack to form the 3D phase, thereby hierarchically self-assembling with correlated phases of the duplex helices into the bulk helical structure [40,41].

2. Results and Discussion

2.1. Helix Pitch and Cone Angle Measurement

The phase behavior of binary mixtures of CB7CB and 5CB was characterized as a function of weight percent 5CB, x , in the range $12.5 < x < 95$, generating the phase diagram of Figure 2a (obtained using differential scanning calorimetry, shown in Supplementary Figure S1). The N–TB phase transition was probed using polarized transmission optical microscopy (PTOM) to observe the various mixtures in untreated and planar cells for x up to 62.5 (Supplementary Figure S2). In the mixtures with $x \leq 25$, the TB phase exhibits the typical stripe texture on cooling, which was shown to be due to a spontaneous undulation with displacement along z of the planes of constant azimuthal orientation φ [42] caused by dilative stress on the helical structure due to the shrinking of p_H on cooling [30]. For $x \geq 37.5$, we found that the stripes form briefly on cooling but that the texture then relaxes into a state of uniform birefringence, indicating that the addition of 5CB fluidizes the phase so that it can anneal into an undulation-free director field configuration [43] (see Supplementary Figure S3). This demonstrates the utility of making mixtures of 5CB with CB7CB to obtain a uniform and undulation-free, well-aligned TB phase. The isotropic (I) to nematic (N) transition temperature of the mixtures, T_{IN} , decreases monotonically as x increases, while the N–TB phase transition temperature, T_{NTB} , decreases nearly linearly with the addition of 5CB until the transition becomes undetectable for $x > 62.5$ (Supplementary Figures S1 and S4). These behaviors are similar to those seen in mixtures of CB9CB/5CB [19] and CB7CB/7OCB [44].

Resonant soft X-ray scattering (RSoXS) at the carbon K-edge, used to carry out direct, in situ measurement of the bulk helical nematic structure in the mixtures [30], exhibits diffraction arcs in the TB phase corresponding to periodicities in the 8–11 nm range. Extensive freeze-fracture studies (see Supplementary Materials) also show the helix pitch p_H , the distance along z for a 2π circuit of the helix, to be in the 8–11 nm range [29]. These observations, discussed further below, lead us to assign the RSoXS diffraction to be from the fundamental periodicity of the helix, i.e., with $q_H = 2\pi/p_H$. In the mixtures, the diffraction arcs are smooth and are relatively narrow in wavevector q at low temperatures, as in neat CB7CB [30], indicating that the pitch is homogenous throughout the sample. As the temperature is raised, the scattering tends to broaden in q into a distribution of individual arcs of differing q_H , including some with linewidths comparable to 0.0002 \AA^{-1} , the wavevector resolution of the diffractometer (Supplementary Figures S5 and S6, and [30]). This behavior is taken as evidence for the development of domains in the sample with a distribution of values of average helical pitch. Detailed studies of neat CB7CB [30] showed that the lower limit of the pitch in the measured distributions was a repeatable function of T but

that the upper limit varied erratically from scan to scan in T , indicating that the TB helix pitch is much softer in response to stretching than to compression and that the stretching is due to non-uniform stress distributions that develop in the macroscopic textures of the helix axis [30]. For this reason, p_H is taken to be the length corresponding to the lowest- q half-height value in each of the measured distributions, as shown in Supplementary Figure S6. The resulting p_H data are plotted vs. reduced temperature $T_{NTB} - T$ in Figure 2b and vs. T in Supplementary Figure S7. As the TB phase of the $x = 0$ and 12.5 mixtures is heated toward T_{NTB} , a coexistence range of T is entered in which some of the TB domains melt. This causes the p_H distribution to narrow at the highest T 's in the TB phase, with the upper limits of the pitch approaching the lower. However, the $x = 25$ and 37.5 mixtures do not exhibit this behavior: the pitch range remains broad near the transition, indicating that the coexistence range is narrower at higher 5CB concentrations, consistent with what we observe using PTOM.

The optical cone angle of the TB helix, θ_H , was determined for the mixtures from measurements of the birefringence, Δn , of the N and TB phases, as detailed in the Supplementary Information (Supplementary Figure S8) [45]. Published values of θ_H from birefringence [45] and NMR experiments [46] are also available for neat CB7CB. The θ_H data are plotted vs. $T_{NTB} - T$ in Figure 2c and in Supplementary Figure S9. The data show that Δn increases continuously on cooling through the N phase, and then near the N–TB transition abruptly begins to decrease. We take this change to indicate the onset of the collective heliconical ordering in the TB phase. The N phase birefringence is somewhat smaller than that of pure 5CB, presumably a consequence of the cyanobiphenyl groups in CB7CB being substantially tilted (by $\sim 30^\circ$, Supplementary Table S1) from the average dimer orientation in the N phase, which is substantial. The development of heliconical ordering then further reduces Δn in the TB phase.

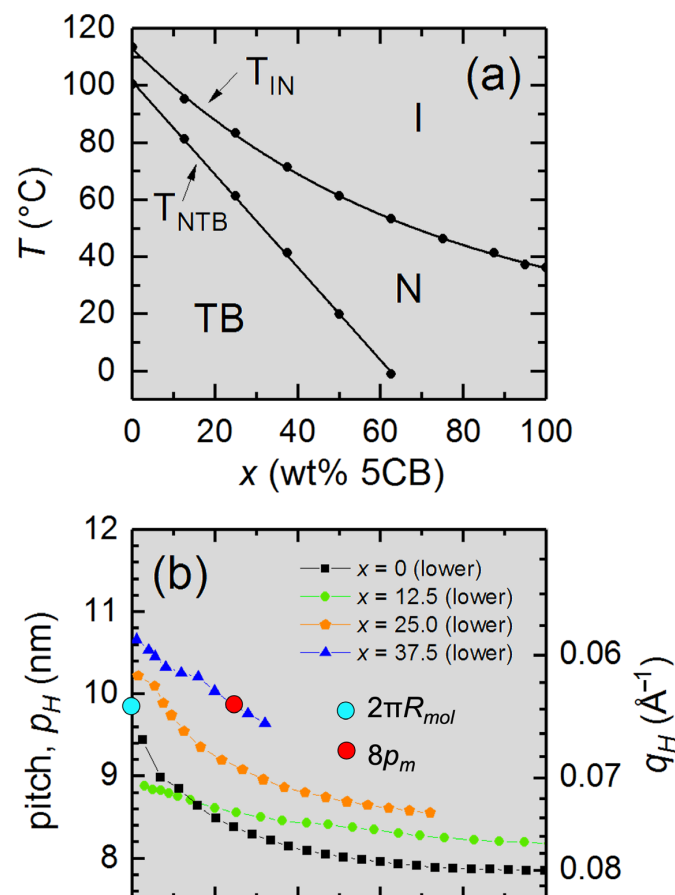


Figure 2. Cont.

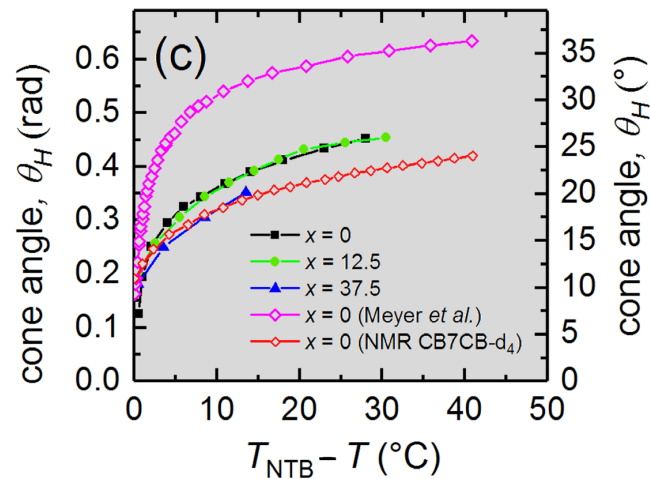


Figure 2. (a) Phase diagram of the CB7CB/5CB mixtures vs. weight %, x , and temperature, T , exhibiting isotropic (I), nematic (N), and twist-bend (also termed heliconical) nematic (TB) phases. (b,c) Helix pitch, p_H , obtained by resonant soft X-ray scattering (RSoXS), and optical cone angle, θ_H , determined from birefringence measurements, of the heliconical structure in the TB phase vs. x and $T_{NTB} - T$, where T_{NTB} is the N–TB phase transition temperature. Birefringence [45] and NMR data [46] from literature sources are also included. In CB7CB, the helix pitch near the transition is found to be $p_H \approx 2\pi R_{mol}$ (blue dot in (b)), where R_{mol} is the bend radius of curvature of an extended CB7CB molecule. Diffuse, non-resonant X-ray scattering indicates periodic segmentation along the helix of spacing $p_m \approx 1.25$ nm. The pitch near the transition has eight such segments (red dot in (b)).

2.2. Bend Deformation and the Geometry of the Twist-Bend Helix

If the heliconical ground state axis of the TB phase is taken to be along z , then $\mathbf{n}(\mathbf{r})$ may be written as

$$\mathbf{n}(z) = (x \sin \theta_H \cos \varphi(z) + y \sin \theta_H \sin \varphi(z) + z \cos \theta_H), \quad (1)$$

where $\varphi(z)$ is the azimuthal angle given by

$$\varphi(z) = q_H \cdot z = (2\pi/p_H)z, \quad (2)$$

as sketched in Figure 1c–f. The heliconical structure can be represented as a rotation on a cone as in Figure 1c or by the green director contour lines in Figure 1e,f, representing the path (contour line) along which the incremental displacement is always along $\mathbf{n}(z)$. The local nematic order tensor is biaxial, with principal axes given by the director (\mathbf{n}), polarization (\mathbf{p}), and auxiliary (\mathbf{m}) unit vectors. We begin by considering the bend deformation of \mathbf{n} , given generally by the director rotation vector

$$\mathbf{B}_n(\mathbf{r}) = \mathbf{n}(\mathbf{r}) \times [\partial \mathbf{n}(\mathbf{r}) / \partial s] \quad (3)$$

where s is the displacement along the contour. Since by definition of the pitch, we have

$$q_H \equiv d\varphi/dz \quad (4)$$

and, from the geometry of the helix in Figure 1f,

$$\cos \theta_H = dz/ds, \quad (5)$$

we find

$$d\varphi/ds = q_H \cos \theta_H. \quad (6)$$

Figure 1f shows the geometry of reorientation on the director contour line of $\mathbf{B}_n(\mathbf{r})$, the bend rotation of $\mathbf{n}(\mathbf{r})$ about auxiliary vector $\mathbf{m}(\mathbf{r})$, and $T_p(\mathbf{r})$, the twist rotation of the biaxial vector $\mathbf{p}(\mathbf{r})$ about $\mathbf{n}(\mathbf{r})$, wherein

$$B_n = \partial n / \partial s = (\partial \varphi / \partial z)(\partial z / \partial s)(\partial n / \partial \varphi) = (q_H \cos \theta_H)(m \sin \theta_H) \quad (7)$$

$$B_H = (q_H \cos \theta_H) \sin \theta_H = (1/R_{mol}) \sin \theta_H, \quad (8)$$

where B_H is the magnitude of the bend B_n of $\mathbf{n}(z)$ in the helix, $B_H = B_n(\theta_H)$.

Additionally,

$$T_p = (\partial p / \partial s)_T = (\partial \varphi / \partial z)(\partial z / \partial s)(\partial p / \partial \varphi)_T = (q_H \cos \theta_H)(n \cos \theta_H) \quad (9)$$

$$T_{BX} = (q_H \cos \theta_H) \cos \theta_H = (1/R_{mol}) \cos \theta_H \quad (10)$$

$$B_H^2 + T_{BX}^2 = (1/R_{mol})^2 = B_{mol}^2 \quad (11)$$

The magnitudes of these deformations, B_H and T_H , are uniform in space and, under the constraint noted above, satisfy the condition $B_H^2 + T_H^2 = 1/R_{mol}^2$, describing the exchange of director bend for biaxial twist as θ_H is decreased, accounting in a fundamental way for the possibility of having a short pitch in the limit of small θ_H .

B_H values calculated using Equation (8) are plotted in Figure 3a vs. $\sin \theta_H$ using the q_H and θ_H data of Figure 2 and vs. temperature in Figure S10. The B_H values fall quite closely onto a straight line passing through the $(B_H, \sin \theta_H)$ origin, indicating that changing T or the 5CB concentration x just moves points along the line, a quite surprising result that enables an immediate prediction: if $B_H(\sin \theta_H)$ is indeed linear in $\sin \theta_H$, then we must have $q_H(\theta_H) \cos \theta_H = S$, the (constant) slope of “the line”. At high temperatures in the TB phase where θ_H is approaching zero, we will have $\cos \theta_H \approx 1$ and therefore $q_H = S$. Thus, for data on the line, the slope of the line should give the limiting helix pitch p_{Hlim} near the N–TB transition as $2\pi/S$. Fitting the B_H data in Figure 3 to a line through the origin yields $S = 0.64 \text{ nm}^{-1}$ and, therefore, $p_{Hlim} = 9.8 \text{ nm}$. This value is plotted as the yellow dot in Figure 3a and is indeed close to the measured pitches at high T in the TB phase, deviating from the maximum pitches of the different mixtures by less than 10%, characteristic of the deviation of the $B_H(\theta_H)$ data from the fitted line, which has p_H increasing weakly with increasing 5CB concentration.

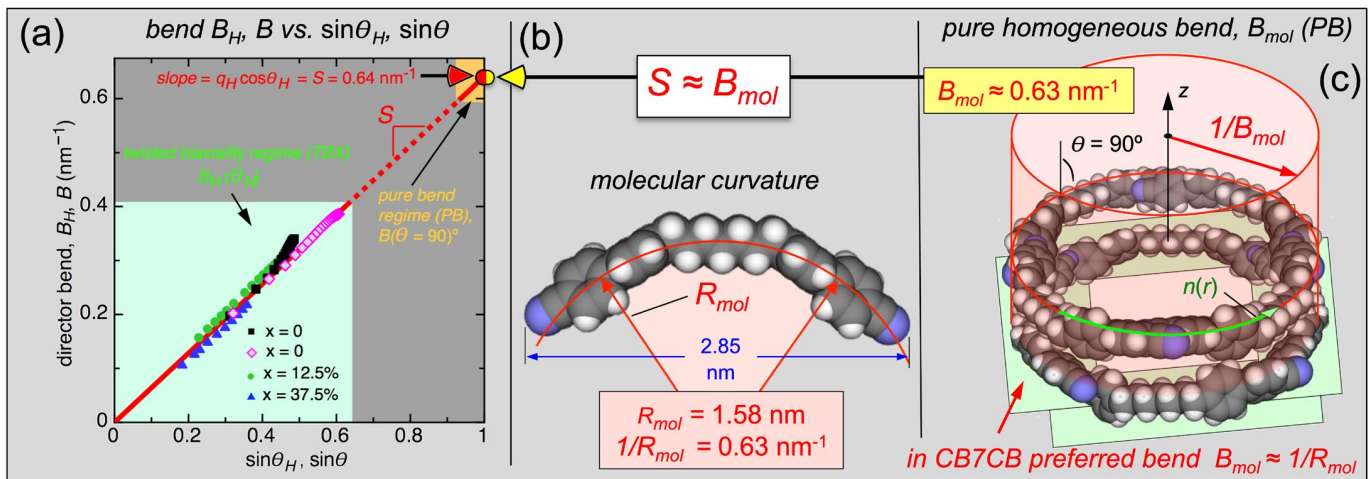


Figure 3. (a) Director bend deformation magnitude $B_H(\theta_H) = (q_H \cos \theta_H) \sin \theta_H$ calculated from the q_H and θ_H data of Figure 2. The measured bend values lie close to a straight line through the origin, indicating that $q_H \cos \theta_H = S$ (slope) = 0.64 nm^{-1} . Changing x or T just moves the points along “the line”. (b) The $B_H(\theta_H)$ data of (a) can be related to the molecular shape of CB7CB by noticing that S is nearly equal to its inverse molecular radius of (bend) curvature $1/R_{mol}$ obtained by fitting atomic centers to a circle. This suggests that the extrapolation to $\theta = 90^\circ$ describes the state of maximum intrinsic bend, obtained by putting the molecules into the state of pure homogeneous bend (PB) as in (c), in a brickwork packing motif, while energetically pinning them to a cylinder of variable radius on which they can seek their intrinsic bend curvature B_{mol} . For CB7CB, which has a bent shape that fits

neatly onto a circle, $B_{mol} \approx 1/R_{mol}$ and the pitch measurements of (a) are described by $B_H = B_{mol} \sin \theta_H$. This relation elegantly connects macroscopic helix characteristics at small θ_H , where the TB structure is dominated by biaxial twist and has little bend, to the bent molecular shape.

The observation that $q_H \cos \theta_H$ is nearly constant leads immediately to the question of how to interpret this fitted value of S . That $B_H = S \sin \theta_H$ means that $S = B(90^\circ)$, the maximum achievable value of bend of $\mathbf{n}(z)$, obtained when θ is extrapolated to 90° . However, in the helix, we also have a director twist of magnitude

$$T_H(\theta_H) = q_H \cos^2 \theta_H, \quad (12)$$

which, if $q_H \cos \theta_H = S$, is given by

$$T_H(\theta_H) = S \sin \theta_H \tan \theta_H, \quad (13)$$

meaning that the twist elastic energy density $U_T = K_T T_H^2 / 2$ grows strongly with increasing θ_H , effectively setting an upper limit of $\theta_{Hmax} \lesssim 35^\circ$ on the physically achievable range of θ_H and making the limit $\theta_H \rightarrow 90^\circ$ non-physical for the TB helix.

2.3. Pure Bend Regime (Hypothetical)

We propose, alternatively, that the extrapolation of $B(\theta)$ to $\theta = 90^\circ$ represents a completely different physical situation, the one exhibiting the maximum preferred bend of $\mathbf{n}(z)$. This must require a geometry: (i) in which there is only director bend (pure bend (PB)), (ii) in which this bend has its preferred value everywhere (constant magnitude of director bend), and (iii) in which $\theta = 90^\circ$, that is $\mathbf{n} \perp \mathbf{z}$. These conditions are uniquely realized in the geometry of Figure 3c, in the system of CB7CB molecules in which their atoms are attracted to a cylindrical surface of variable radius, packed, and equilibrated. At low temperatures, this condition maximizes the number density, a condition explored by packing DFT-based (DFT/B3LYP/6-31G**) space-filling models of rigid all-trans CB7CB. Maximum density in a pure bend geometry is achieved when the molecules are arranged with $\mathbf{B}(\mathbf{r})$ and $\mathbf{n}(\mathbf{r})$ parallel to the x - y plane ($\theta = 90^\circ$) and on the cylinder of preferred radius $1/B_{mol}$. Since the shape of an extended CB7CB molecule matches a circle reasonably well, the preferred PB radius can be estimated from the construction shown in Figure 3b, which minimizes the mean square atomic distance from a circle by varying the circle radius R_{mol} . That is to say, for CB7CB, we take the preferred bend B_{mol} in Figure 3c to be the inverse of the molecular radius of curvature R_{mol} , indicated in Figure 3b. The resulting effective molecular radius of curvature of CB7CB is found to be $R_{mol} = 1.58$ nm. This corresponds to a molecular bend of $B = 1/R_{mol} = 0.63$ nm⁻¹, which is remarkably close to the slope $S = 0.64$ nm⁻¹, independently derived in Figure 3a from the θ_H, p_H data. These data are plotted in Figure 3a, with S as the red half dot and B_{mol} as the yellow half dot at $\theta = 90^\circ$, where $B(\theta)$ extrapolates to S .

Remarkably, we find that the B_H vs. $\sin \theta_H$ trajectory of the data in Figure 3 apparently could have been predicted from the molecular quantity, R_{mol} , even at small θ_H where there is little director bend left in the structure, and, furthermore, that the limiting pitch at the N-TB transition can be given in terms of the molecular quantities as $p_{Hlim} = 2\pi/S = 2\pi/B_{mol} = 2\pi R_{mol} = 9.8$ nm. That is, if the TB system B_H vs. $\sin \theta_H$ trajectory has slope B_{mol} , meaning that

$$q_H \cos \theta_H = B_{mol}, \quad (14)$$

then the helix pitch at $\theta_H = 0^\circ$ is just the circumference of the circle in Figure 3b,c, describing the molecular radius of bend curvature, R_{mol} . This circumference accommodates about four CB7CB molecules of all-trans length (~ 2.8 nm) with a slight overlap of the CN groups (Figure 3c).

Thus, if the rationale for the twist-bend phenomenon is based on the effects of molecular bend, then this observation suggests that the $q_H(\theta_H)$ data respond to changes of temperature and concentration by moving on the trajectory $B_H \approx S \sin \theta_H$, which is, in turn,

being controlled through S by molecular bend by way of R_{mol} , even at small θ_H . This result is also surprising because, for TB phases and especially near the N–TB transition where θ_H tends to be the smallest, there is little director bend left in the structure, the bend magnitude $B_H(\theta_H)$ being quite small, as shown in Figure 3. Nevertheless, if the B_H vs. $\sin\theta_H$ data are on the line, the bend is still proportional to B_{mol} . Thus, the data of Figure 3 indicates that the structural preference for the TB ordering to give a well-defined q_H is not a preference for constant bend. Several recent studies analyzing the elasticity of the TB helix pitch have found the director curvature bend energy to be orders of magnitude too weak to account for the observed TB pitch compressional elastic constant, C , measured as θ_H becomes small, and were led to propose local lamellar smectic positional correlations as an alternate source of rigidity [21,47]. Figure 3 shows, however, that since the data are nearly on the line, the helix pitch appears to be controlled by molecular bend, even in the absence of director bend at small θ_H .

2.4. Polygon Chain Model

These considerations lead next to the question of the geometrical meaning of “the line” and, in particular, the relationship

$$d\varphi/ds = q_H \cos\theta_H = B_{mol}. \quad (15)$$

Thus, on the line, for different values of θ_H , q_H is such that $s(\Delta\varphi = 2\pi)$, the net distance traveled along the director contour path for a 2π increase in φ (one complete turn of the helix, shown as the black dashed line in Figure 1e), is independent of θ_H , and furthermore given by

$$s(\Delta\varphi = 2\pi) = 2\pi/B_{mol} = 2\pi R_{mol} \quad (16)$$

for all θ_H , including the PB regime $\theta = 90^\circ$ (the path through $\Delta\varphi = 2\pi$ around the circle of circumference $2\pi R_{mol}$). This invariance does not appear to be a symmetry of the system because the TB ground state at small θ_H is entirely different from that of the PB at $\theta = 90^\circ$. However, this is clearly the condition that connects the two regimes.

We can shed light on this condition by developing a geometrical model, the rectangle-triangle (RT) polygon chain, sketched in Figure 4, that, by design, exhibits $s(\Delta\varphi = 2\pi) = 2\pi R_{mol}$ over the entire range of θ_H . This model is an assembly of rectangular and triangular plates connected into a periodic chain where the lines representing shared edges of rectangles and triangles are bendable hinges. The rectangles are attached to, and constrained to be locally parallel to, a flexible rod in the form of a helical spring representing the contour line of the director (green lines, Figures 1e,f and 4b) on a cylinder of tunable radius $R = R_{mol}\sin\theta_H$. The corresponding tunable pitch, $p_H = 2\pi R_{mol}/\cos\theta_H$, guarantees that such a chain of length $s(\Delta\varphi = 2\pi) = 2\pi R_{mol}$ (in the example shown in Figure 4b, this length corresponds to eight rectangles, $8L$) always makes exactly one turn of the helix. The helical rod is inextensible, enforcing by construction the condition that $s(\Delta\varphi = 2\pi) = 2\pi R_{mol}$. In the basic structural unit of the chain, consisting of two rectangles and a 45° isosceles triangle, a 45° bend in the director is enforced by the triangular hinge when the triangle and rectangles are all in the same plane, the condition at $\theta = 90^\circ$ where the whole construction lies parallel to the x - y plane (Figure 4b). This directly models the molecular organization of the PB limit in the cylindrical shell packing of Figure 3c.

The hinge angle $\beta_0 = 45^\circ = 360^\circ/8$ was chosen because, as discussed below, a diffuse feature in the non-resonant X-ray scattering in the TB phase indicates that there are ~ 8 molecular half-lengths in the TB pitch at small θ_H . Since the B_H values fall on “the line” in Figure 3a, there must correspondingly be in the PB regime ~ 8 segments around the $2\pi R_{mol}$ circumference. Indeed, as shown in Figure 5a, the PB regime is well modeled by the arrangement of four 45° bent rod molecules. We propose that each ring in this structure is stabilized by neighboring rings in an arrangement where adjacent rings have a difference in azimuthal orientation of 45° , such that the flexible molecular centers in one ring are over the regions of fluctuating end-to-end molecular contacts in the neighboring ring, an

entropically favored association. This makes a construction like a cylindrical brickwork chimney, as discussed in the next section. With this choice, eight rectangle, long edges must make a complete turn, so the rectangle length, L , is chosen such that $8L \sim 2\pi R_{mol}$. The corresponding magnitude of the director bend is then

$$B = (\pi/4)/L = (2\pi)/8L = 1/R_{mol} = B_{mol}. \quad (17)$$

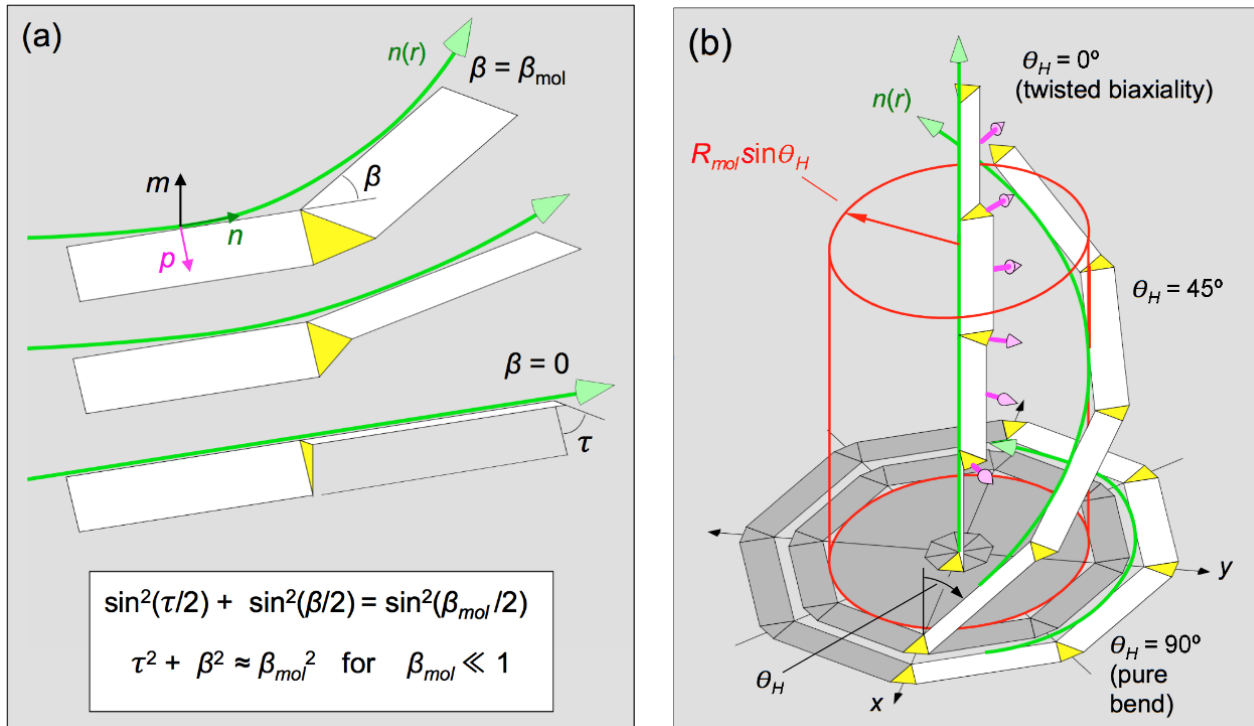


Figure 4. A polygon chain that models an elastic band that freely interconverts between director bend and biaxial twist. This chain quantitatively embodies the geometry of the TB helical state as manifest in the relationship $B(\theta_H) = (1/R_{mol})\sin\theta_H$ from the plot in Figure 3a and motivates our picture of the TB phase as an assembly of sterically stabilized, oligomeric chains. (a) In this geometry, the rigid triangular and rectangular plates form a chain by sharing common edges, which are flexible hinges, enabling the chain to twist if its bend is reduced, as sketched and described geometrically by the relationship indicated in the inset. (b) The polygon chain is attached to a helical rod that is flexible but of fixed length $2\pi R_{mol}$, which can be made to change its pitch by sliding its upper end along z . Here, only a half-period of the helix is drawn. The red cylinder changes radius as $\sin\theta_H$ to keep the rod length constant. In its flattened state ($\theta_H = 90^\circ$), the chain models directly the PB regime in Figure 3c, in this case with eight segments and eight 45° bends. If θ_H is reduced, then this structure rigorously maintains the conditions $q_H(\theta_H)\cos\theta_H = 1/R_{mol}$, and $B(\theta_H) = (1/R_{mol})\sin\theta_H$, i.e., it moves on “the line” like the B_H vs. $\sin\theta_H$ data in Figure 3a. In the fully stretched out state ($\theta_H = 0^\circ$), the twisted biaxiality (TBX) regime, the director bend is replaced by the twist of the biaxial vector \mathbf{p} (magenta arrows), with a pitch $p_H = 2\pi R_{mol}$ mediated in eight twist steps of 45° each, as suggested by non-resonant X-ray scattering data.

The helix can be tuned by pulling the ends of the rod so that they become separated along a line parallel to z ; the separation being the pitch, p_H , as indicated by the black arrow in Figure 1e, which decreases θ_H and makes the rod less bent everywhere along its length. The bend angle, β , of the local elements, thus decreases from the maximum of $\beta_o = 45^\circ$ causing them to buckle, the triangle swinging out of the plane of the rectangles to cause less bend, and in the process, inducing a local relative twist τ of the rectangle planes, which are free to rotate about the rod axis, as sketched in Figure 4a. With this geometry, if the tilt of $\mathbf{n}(z)$ relative to z is θ_H , then the angle between the triangle and rectangle planes will

be $-\theta_H$, the condition that keeps the triangle planes always parallel to the x - y plane. If the separation of the rod ends is increased and p_H approaches the rod length $2\pi R_{mol}$, then $\theta_H \rightarrow 0$, $B_H \rightarrow 0$ as $B_H = \sin\theta_H/R_{mol}$, and the rod becomes nearly straight, with the local geometry changing as shown in Figure 4a. The triangle plane is eventually oriented normal to the rod, and its initial induced bend in the rod of $\Delta\varphi = 45^\circ$ is now completely converted to an induced local relative twist about the director of the rectangle plane normals through $\Delta\varphi = 45^\circ$ at each hinge, as illustrated in Figure 4b. The bend angle, β , twist angle, τ , and β_{mol} are geometrically related, as indicated in Figure 4a.

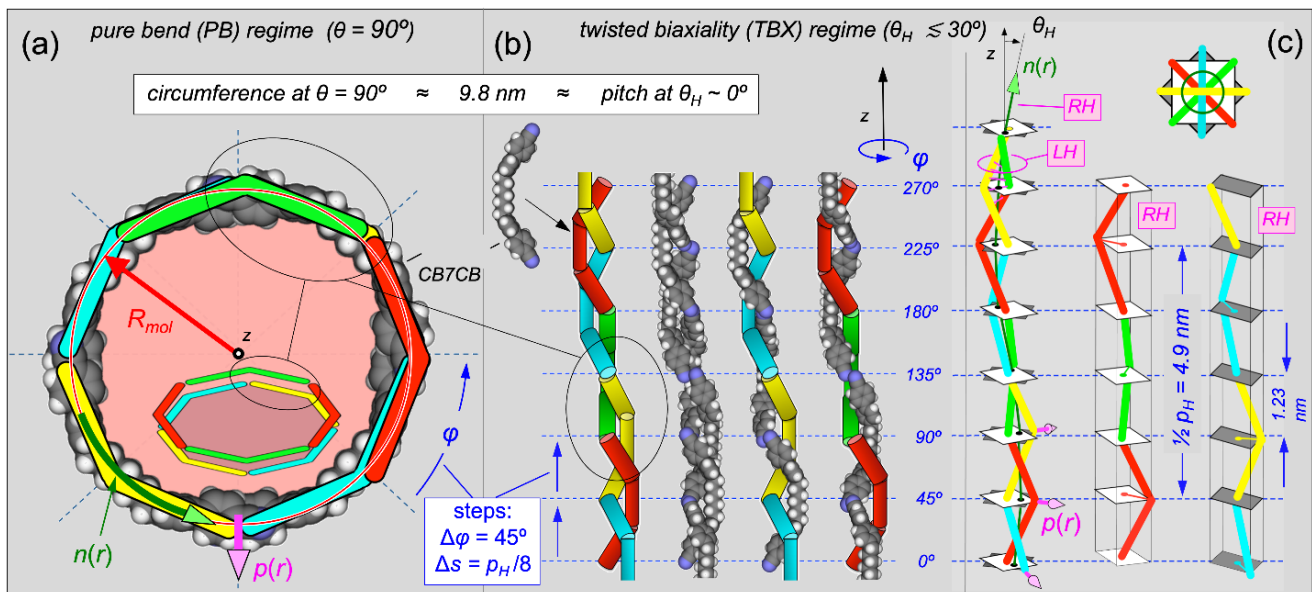


Figure 5. Realization of the polygon chain model for discrete molecules, modeling CB7CB by bent rods. Oligomeric chains are formed in both the PB and TBX regimes by the brickwork tiling of half molecules, with a repeat distance indicated by the blue dashed lines, corresponding to the short-range periodicity observed in diffuse, non-resonant X-ray scattering (Supplementary Figures S11 and S13). Each segment contains a pair of half-molecules. This tiling is stabilized by the entropic association of molecular ends and CB7CB's flexible center. The constraint of the bend data and the polygon chain model is that the helix pitch p_H at small θ_H in the TBX regime is the circumference of the circle in the PB regime. Since p_H at small θ_H is 8 segments in length, the change in φ per segment is taken to be 45° in both the PB and TBX regimes. (a) PB regime showing the brickwork tiling of molecules as in Figure 3c: two chains of 45° bent molecules (red-green, yellow-cyan) forming eight segments of half-molecule pairs, with angular bend jumps of $\Delta\varphi = 45^\circ$ between each pair, and a $\Delta\varphi = 45^\circ$ phase difference in the orientation of the two chains. The small inset shows an oblique view of the packing structure. (b,c) Oligomeric chain structure showing bent-rod and molecular models of the brickwork tiling in the TBX regime: two chains of 45° bent molecules (red-green, yellow-cyan) forming eight segments of half-molecule pairs, with angular biaxial twist jumps of $\Delta\varphi = 45^\circ$ between each pair, and a $\Delta\varphi = 45^\circ$ phase difference in the orientation of the two chains. The two right-handed (RH) chains associate to form a left-handed (LH) double helix. (c) For uniaxial half-molecules, the optical polarizability of a given segment can be obtained geometrically. The optical cone angle is $\theta_H \sim 10^\circ$ for the structure drawn, the case where the molecular planes are untilted.

The rectangles also represent the principal axes of the local biaxial nematic ordering tensor of the director field (director n , flexoelectric polarization direction p , auxiliary unit vector m), as in Figure 4a. Thus, as θ_H increases, the overall structure of a single pitch is converted from the $\theta_H \sim 90^\circ$ state: a series of eight steps of 45° rotation of director bend and of local biaxiality about its m axis on the circumference of the circle of radius R_{mol} ; to the $\theta_H \sim 0^\circ$ state: a series of eight steps of 45° twist rotation of the local biaxiality about its n axis, on a path along z of length $2\pi R_{mol}$. This scenario precisely maintains $q_H \cos\theta_H = B_H$

throughout the range of q_H , i.e., puts B_H vs. $\sin\theta_H$ on “the line” (Figure 3a). We denote these ranges of large and small θ_H , respectively, as the pure bend (PB) regime ($\theta_H \sim 90^\circ$) and the twisted biaxiality (TBX) regime. The RT model directly shows that the structural stability of the local elements through the transition from pure bend to twisted biaxiality is what is required to maintain the compressional elasticity of the pitch under the condition that $B_H \rightarrow 0$ and director curvature elasticity drops out. Actual twist-bend phases typically have $\theta_H \lesssim 30^\circ$, so they are much closer to the twisted biaxiality limit than the pure bend. Thus, in “TB”, the twist should be taken to mean the twist of biaxiality. The $\theta_H \sim 0^\circ$ regime represents the state of the helix dominated by twisted biaxiality but having no macroscopic optical tilt. Such a state is achievable, as shown below. In the CB7CB mixtures, the TB phase appears to come in with a small but finite θ_H , consistent with the optical, X-ray, and DSC evidence for a first-order N–TB transition.

The RT model can be made for any angle β_{mol} . If β_{mol} is small, then

$$\tau^2 + \beta^2 \cong \beta_{mol}^2, \quad (18)$$

with β and τ becoming the orthogonal projections of a vector of magnitude β_{mol} , constrained to move on a circle (Figure 4a). In the limit that $\beta_{mol} \rightarrow 0$ with L/β_{mol} constant and assuming that the hinge bends remain highly flexible, the RT chain becomes like a sheet of paper bent into the accordion fold of a fan, with high bending rigidity in the radial direction, and low bending rigidity in the circumferential direction. Upon pulling the bend out, such a sheet will exhibit little elastic resistance against conversion from continuous bend to continuous twist. In the continuum limit

$$B_H^2 + T_{BX}^2 = B_{mol}^2 = B_H^2 = \beta_{mol}^2/L^2, \quad (19)$$

a result that is also derived in Figure 1f from the projective geometry of the helix. The balance of bend and twist is controlled by B_{mol} even in the limit of zero bend ($T_{BX} \cong B_{mol} - B_H^2/2B_{mol}$).

2.5. Steric Oligomerization of Bent Molecular Dimers

In the RT model, the constraint that $q_H \cos\theta_H = B_{mol}$, independent of θ_H , is built into the model by the fixed length of its chain of polygons, a condition that would seem most applicable to a system of locally bent flexible oligomer or polymer chains. In the dimer TB phases considered here, there are no chemical links between molecules, so it is necessary to understand, in the context of independent bent molecules, how such a similar, polymer-like condition could come about in both the PB and TBX regimes, how the PB and TBX regimes are linked, and, therefore, how biaxial twist in the absence of bend comes to be controlled by B_{mol} .

We propose that molecular bend and steric packing constraints of the condensed TB phase combine to stabilize oligomeric chains of molecules and that the brickwork packing motif, introduced in Figure 3c and detailed in Figure 5a, is the common structural feature that stabilizes the chains and connects the PB and TBX regimes. The brickwork packing of a pair of adjacent chains can be visualized as a string of segments, each containing a pair of oppositely directed molecular halves linked by interfaces, each containing the center of a molecule in one chain and the tails of two in the other. This motif has also been found in other molecular dimer liquid crystal structures [48]. This assembly is stabilized by the well-known tendency for rigid and flexible molecular subgroups to nano-phase segregate [49], with the flexible molecular centers most readily accommodating the fluctuations in a relative position of neighboring molecular ends or tails. We refer to a double helix chain formed in this way as a duplex helical tiled chain (DHT chain, DHTC). The intra-duplex tiled linking is responsible for the apparent fixed contour length, $s(\Delta\varphi = 2\pi) = 2\pi/B_{mol}$ along $\mathbf{n}(r)$, and manifested in the construction of Figure 4.

This proposal is supported by the observation of a diffuse, non-resonant X-ray scattering feature in the N and TB phases of pure CB7CB, having a peak on the q_z -axis at

$q_m \approx 5.05 \text{ nm}^{-1}$. A similar peak is found in the N and/or TB phases of a variety of other bent molecular dimers, with q_m in the range $4 \text{ nm}^{-1} < q_m < 5 \text{ nm}^{-1}$ [14,15,19,22,23,31,50,51], as discussed in Supplementary Figures S11–S13. The typical appearance of this TB phase feature is shown in Figure S11, which plots the non-resonant X-ray structure factor of the TB phase in CB7CB, calculated from the molecular dynamics simulation in the TBX regime reported previously [29]. The white ellipses indicate the on-axis peaks, which can also be seen in Supplementary Figure S13, which plots z-axis intensity scans $I(q_z)$ of CB7CB [15] and of a DTC5C7/DTCSe mixture [31]. These scans indicate a periodic electron density modulation and, therefore, molecular positional ordering along the helix with a fundamental periodicity of $d_m \cong 1.25 \text{ nm}$, consistent with the presence of short-ranged periodic positional correlation of similarly structured molecular segments along z. This finding supports the brickwork association proposal since this value of d_m is close to half of the molecular length $M = 1.4 \text{ nm}$ of extended CB7CB, which is what required for the segment length in a brickwork tiling. In fact, a comparison of d_m with the extended molecular length for the bent molecular dimer systems for which d_m data is available noted earlier in this paragraph, shows that the condition $d_m/M \sim 1/2$ appears to be a general trend, as illustrated in Supplementary Figure S12. In CB7CB, since d_m is comparable to $p_H/8 = 1.22 \text{ nm}$, it is close to the brickwork segment length in the PB regime on the R_{mol} circle (Figure 5a), an observation that can be taken as evidence for there being similar segments at small θ_H .

We made an initial evaluation of whether the peak at q_m (the chain segment scattering) could be understood on the basis of a model in which the self-assembly of a pair of molecular chains is described as a periodic chain of half molecule-long segments, each connected to an adjacent segment by a nearest-neighbor harmonic spring. The structure factor of this standard model for 1D positional ordering exhibits only short-range order at finite temperature [52,53], as described by the monotonic increase in the mean square of fluctuations in the dynamic separation of pairs of elements of the chain with increasing mean separation:

$$\langle (u_0 - u_n)^2 \rangle = \langle \delta u_n^2 \rangle = \sigma^2 n, \quad (20)$$

where n counts the segments along the chain. The 1D structure factor $I_{1D}(q_z)$ fits the data for CB7CB [15] and the DTC5C7/DTCSe mixtures [31] quite well (Supplementary Figure S13), giving, in both cases, a distance along the chain of ~ 15 segments for translational order to be lost, i.e., where $\sqrt{\langle \delta u_n^2 \rangle}$ becomes equal to the segment interval d_m .

Another common feature of the chain segment scattering, $I(q_z, q_\perp)$, in the materials listed in Supplementary Figure S12 is that the width of the diffuse peak in the direction normal to the helix axis z, δq_\perp , is significantly larger than δq_z , its extent along the helix, as seen in Supplementary Figure S11. In some cases, this appears to be mosaically broadening due to alignment defects, but in the TB phase in the DTC5C7/DTCSe mixtures [31], for example, the narrow angular width in q of the resonant q_H peaks shows that the sample is well aligned, and therefore that the broadening of $I(q_z, q_\perp)$ in the q_\perp direction is intrinsic. The corresponding correlation lengths, ξ_\perp and ξ_z , have the inverse relationship, implying that the correlation volumes giving the diffuse non-resonant scattering are extended along z, i.e., a chain-like periodicity along z rather than layer-like correlations.

2.6. Duplex Helical Tiled Chain (DHTC) Structure of the Twist-Bend Phase

The challenge then is to develop a model of the TB helix with small θ_H in which it is made up of at least pairs of molecular chains in a brickwork tiling with subsections along z of pairs of antiparallel half-molecules, in which, for CB7CB, the structural twist between segments is 45° . To this end, we considered the organization of single-stick and space-filling molecular models consistent with the above requirements. The PB regime is readily modeled by the packing of all-trans space-filling models of CB7CB and, as in Figure 5, by either two- or three-segment bent stick models having 45° or 30° bend, respectively. In the PB limit, brickwork tiling of either stick model gives a bend of 45° per segment and four molecules per ring (Figure 5a) so that the change in azimuthal orientation φ is 45° per segment.

The required structures are shown in various representations in Figures 5b,c and 6, and Supplementary Figure S14. The basic structural associations are of three molecules like that of the green, cyan, and yellow groups inside the black elliptical rings in Figure 5a,b, wherein terminal groups of the cyan and yellow tuck into the volume of hard-to-fill space vacated by the bending of the green and can associate with the flexible central aliphatic linkers. This scenario is repeated for the next segment along z , among a group rotated through 45° relative to the initial one and having the cyan molecule in the center, and so on for all z . The stick models in Figures 5b,c and 6 show that this structure is double-helixed, made up of two identical right-handed helical chains of molecules, each transforming into the other by a translation of a single segment length followed by a 45° rotation in azimuthal angle. The paired assembly of two chains is stabilized in both the PB and TBX cases by a combination of a constraint, in the former to be on the cylinder or in the latter to be in a tube created by neighboring chains and by the pressure exerted by the neighboring molecules. In the pairing of the single-strand chains, the overlaps stabilize the structure and the interlocking bends promote the filling of space. In the bent stick representation of Figure 5c, the half-molecular rods can be taken to represent the principal axes of the halves of the molecule. Taking the half-molecule polarizability to be uniaxial, the effective optical anisotropy of a segment of the double helix can be obtained using the construction in Figure 5c. Here, the white square at each level is marked with a black dot that marks the midpoint between the intersections of the two chains with the square. The dark green line connects the midpoints from square to square. Thus, in a given segment, the green line construction will give the orientation of the local principal axis of the average dielectric tensor with the largest refractive index, which we take to be the local director. Thus, the green line represents the trajectory of the optical $n(r)$, which is also a right-handed helix. This construction shows that, in a given segment of the DHT chain, the tilts of the half-molecular optic axes away from z , in this case by $\sim 22^\circ$, tend to cancel one another, leaving a much smaller effective optical helical cone angle, in this case $\theta_H \sim 11^\circ$. The magenta labels in Figure 5c indicate the handedness of the various helices, with the single chains and the director helix being right-handed (RH). Interestingly, the double helix is left-handed (LH).

For clarity, the molecules in Figure 5 are positioned with more symmetry than they will actually have in the typical case. Generally, the planes of the bent molecules in the helices of Figure 5b,c will be tilted away from z through an angle, ψ , as shown in Figure 6 and in Supplementary Figure S14 for both signs of tilt from z . The untilted case could occur at some particular temperature, like the unwinding of the helix in a chiral nematic at a particular temperature.

Figure 6 presents the fully formed DHTC structure in the pure TBX limit for which the optical director tilt $\theta_H = 0^\circ$. In this structure, the projection of the halves of a given tilted molecule onto the x - y plane has an opening angle between them of 45° (Figure 6c), the same as the rotation $\Delta\varphi = 45^\circ$ per segment. This condition requires a tilt of the molecular plane from z of 9.9° . In this case, the two molecular halves in a given segment have parallel projections onto the x - y plane (Figure 6a,c). Since they also have equal and opposite tilts, there must be a principal axis along z of their average biaxial contribution to the dielectric tensor (Figure 6d). Starting from this structure, a helical director field of finite θ_H can be generated by changing the molecular tilt (Supplementary Figure S14) or by helical deformation of the DHT chain (Supplementary Figure S14). Introducing a director bend into the DHT chain reduces biaxial twist, following the geometric projection scenario of Figure 3f and of the RT model in Figure 4. This comes about as illustrated in Figure 6d,e, showing that, on the boundary between the two duplex chain segments containing the halves of the red molecule (denoted by a black circle), the projections of the halves of its cyan and yellow molecular neighbors make a 45° angle to one another. As indicated in Figure 6d, this corresponds to twist $\tau = 45^\circ$ for $\beta = 0$ at a yellow triangle in Figure 4a. In the presence of director (heavy green line) bend, β , the rotation of these neighbors relative to the red molecule is of opposite sign ($+\beta/2$, $-\beta/2$) and applied on the projections, as on

the edges of the yellow triangle, causing the black disc plane, with application of bend, to rotate about p , remaining, as in Figure 6b, coplanar with the yellow triangle as it reorients (Figure 4a). Elastic deformation of the DHT chain then satisfies the RT model constraints, which put $B_H(\theta_H)$ on “the line” in Figure 3a. With Equation (10), we have

$$B_H = B_{mol} \sin \theta_H, \quad (21)$$

$$T_{BX} = B_{mol} \cos \theta_H, \quad (22)$$

and

$$B_H^2 + T_{BX}^2 = B_{mol}^2. \quad (23)$$

For B_H small, then, the reduction in biaxial twist is controlled by B_{mol} , with

$$T_{BX} \approx B_{mol} (1 - B_H^2 / 2B_{mol}^2). \quad (24)$$

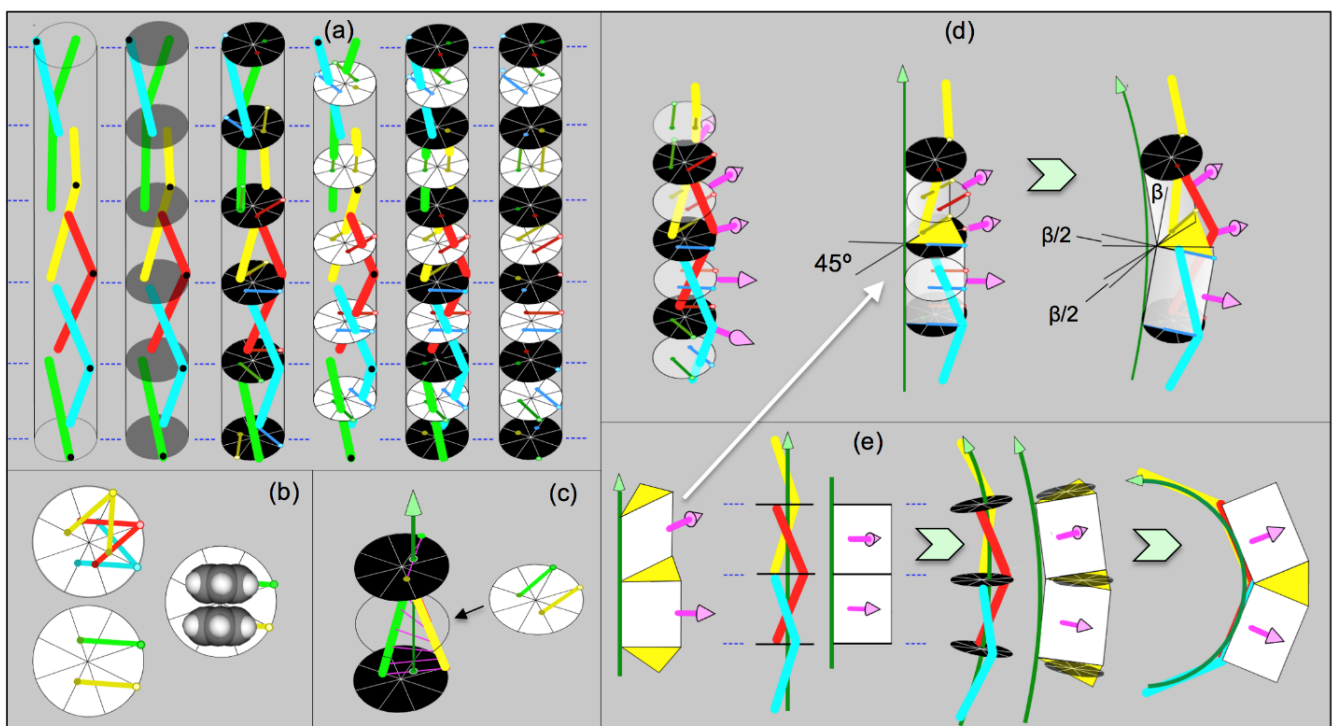


Figure 6. Representation of the TBX regime oligomeric chain structure for $\theta_H \sim 0$, i.e., with $n(z)$ parallel to z . (a) White circles show the projections onto the x - y plane of half-molecules in each segment, and the black circles the projections of half-molecules on to the interfaces between segments. (b) The planes of the 45° bent molecules are tilted from z by an angle ($\sim 10^\circ$) such that the half-molecule projections on the x - y plane are separated by $\Delta\varphi = 45^\circ$, matching the reorientation in successive segments (cyan, red, yellow). This results in parallel chain projections within the segments (yellow, green). This drawing is proportioned with respect to the diameter of the chains according to the molecular volume of 0.76 nm^3 . The segments are 1.23 nm along z and 0.88 nm in diameter, that of the black and white circles. The phenyl ring profiles are on the same scale. (c) When biaxial optical polarizabilities with parallel projection are added, they give an untilted biaxial average ($\theta_H \sim 0$). (d,e) Mating of the polygon chain model with the brickwork oligomeric chain. The projections of the half-molecules onto an interface form a 45° angle that matches that of the yellow triangles in Figure 4. If the oligomeric chain is bent, its black disc, representing the interface between two segments, tilts but remains parallel to the yellow triangle. Thus, in the oligomeric chain, even at small θ_H , the condition $q_H \cos \theta_H = 1/R_{mol}$ is enforced, keeping B_H in Figure 3a on “the line”.

In the limit of large bend, twist is eliminated, and the structure evolves toward the PB limit (Figure 6e).

It is useful here to recall Ref. [16], in which we reported the TB phase in the mesogen UD68, a rigid-core molecule in the form of a $\sim 120^\circ$ bent rod with unequal-length arms. This phase appears to be in the TBX regime, in which case the structure of Figure 6 may be applicable, with one small change, to describe this TB phase, namely that the spacing between black discs would alternate from one pair to the next, between the short-arm length and the long-arm length.

2.7. Three-Dimensional Helical State

The bulk TB phase is a 3D space-filling packing of DHTCs. The overall orientational ordering with uniaxial positive birefringence means that the DHT chains are generally running parallel to one another, making the TB a hierarchical nematic self-assembly of anisotropic, self-assembled oligomeric chains. In the packing of cylindrical objects that are helically modulated, the helical contours on adjacent facing cylinders cross each other (like the stripes on a pair of parallel barber poles of the same handedness if put into contact). This geometry tends to suppress melding of the chains and to maintain the cylinders as distinct entities in the packing. Each DHT chain is then effectively confined to an on-average cylindrical hole in the fluid by its neighboring chains, which exert an effective pressure like that coming from osmotic pressure in a depletion interaction. This picture is supported by the experimental finding that the $B_H(\theta_H)$ data of all the mixtures lie on the same line in Figure 3a, indicating that they behave as if they all have the same B_{mol} (at $x = 37.5$ we might have expected a significant dilution effect leading to a smaller B_{mol}). The constancy of B_{mol} suggests that in the structures determining the pitch, the DHT chains, in the case of the TBX, are comprised dominantly of the bent dimers and that the 5CB is a filler in between. The 5CB dilution lowers the phase stability and reduces θ_H , but this all occurs with $q_H \cos \theta_H = B_{mol}$, implying chains under the same constraint: $d\varphi/ds = B_{mol}$.

Next, we consider the steric packing of the DHT chains that make up the bulk phase. The fact that the resonant X-ray scattering from the bulk TB exhibits diffraction spots from oriented domains that are 3D smectic-like, that is, having resolution-limited width in δq_z , indicates that the long-range ordered pseudo-layer scattering objects are arrays of lamellar sheets extended in the in-plane direction [30,31]. This means that in the bulk TBX packing, the phase φ of the twist in a DHT chain must become coherent with that of its neighbors, a condition that has been observed in nematic phases made by packings of chiral particles internally structured as a steric repulsive helical object, realized, for example, in suspensions of helical flagella [40] and in the extensive simulations of steric helices of Kolli et al. [41]. The existence of the DHT chains opens up the possibility of a number of other arrangements of these objects such that, for instance, it is feasible to observe a transverse twisting of these DHT chains akin to a TGB* phase in some range of parameters. Another example relevant to the TB phase is the helical nanofilament phase found in neat bent-core systems [9,54] in which chiral filamentous bundles of a few smectic layers achieve macroscopic phase coherence of their twist solely by interacting through their periodic biaxiality.

The Kolli simulations appear to be particularly applicable to describe the interaction of, and the potential of, long-range phase ordering for, the DHT chains for finite θ_H in the TBX regime. Supplementary Figure S15 shows an example of the systems of interacting particles employed by Kolli et al. [41], composed of rigid helical chains of contour length, L , made of truncated hard spheres of diameter, D . Comparison of the Kolli particles with the steric shape of the DHT chains of CB7CB, made in Supplementary Figure S12 for the $\theta_H = 10^\circ$ case in Figure 5b, shows particles with helical radius $r/D \approx 0.2$ and pitch, $p \approx L \approx 10D$ match the CB7CB DHT chains quite well. The Kolli et al. phase diagram for $r/D = 0.2$, also reproduced in Supplementary Figure S15, shows that particles having $r/D = 0.2$ systematically give I, N, TB, and smectic phases, with the TB range decreasing as the pitch becomes comparable to

and longer than the particle contour length. Thus, the single-pitch duplex CB7CB chains should be able to order into a 3D TB phase if sufficiently long and rigid. The TB range in Supplementary Figure S15 is limited with increasing volume fraction by the appearance of smectic ordering, corresponding to the positional ordering of the particles into smectic layers of thickness comparable to their length. In the case of living polymer chains, like what we propose for CB7CB, the effective particles will be transient and polydisperse, the latter condition well known to strongly suppress smectic ordering [55], an effect which may expand the TB range.

For $p \approx L$ and $r/D = 0.2$, the Kolli et al. helical particles behave as if they are smooth, like those of Barry et al. [40], which have helical glide symmetry. In these cases, if the steric helical interaction is reduced, for example, by reducing r/D or making $pitch/L$ large, the system will revert to a simple nematic or smectic phase. However, the DHTCs are not smooth but are periodically structured with a local biaxial shape, so the role of variations of the steric shape along the DHT chain must also be considered. Figures 4b, 5c, 6, S11, S15 and S14 all exhibit aspects of the biaxiality of the DHT chains. Figure 4b for the $\theta_H = 0^\circ$ case and Figure 5c show that the projection of the segments onto the drawing plane varies in effective shape along the chain, with a period equal to half that of the helix. This variation is also evident in the projection of the steric shape of a duplex chain in Figure S15. Generally, each segment is biaxial, with a steric cross-section in the x - y plane that has the symmetry of an ellipse. This elliptical shape rotates in azimuthal angle φ along the chain (biaxial twist), as in a twisted ribbon of zero net local curvature, with a period of $p_H/2$, equal to four segment lengths, as is clear in Figure 4b. In the TBX limit, this is the only periodicity of the DHTC. In a dense packing of the DHTCs, steric variations in shape, especially periodic ones, will lead to the development of correlations between chain positions along z . This will be an especially strong effect if the oligomerization has substantially reduced the translational entropy for displacement along z . In the helical nanofilament case [10,54], where the structural periodicity is the helix half-pitch, and the filament steric profile is almost circular, such that the neighboring filaments only weakly sense each other's grooves, the filaments have a strong tendency to order with their biaxial twist in phase. In the DHTC case, sufficiently large ellipticity and packing density will lead to a 3D structure in which adjacent duplexes will align out of phase to facilitate packing. Twisted ribbons, for example, pack best when shifted by a quarter of their pitch.

2.8. Resonant Soft X-ray Scattering as a Probe of the Duplex Helical Tiled Chain Model

Given that we now have a fairly detailed structural model, we reconsider RSoXS as a probe of the helical structure of the TB phase. Interestingly, the first application of resonant scattering to LCs was to probe the helical molecular orientational ordering in chiral tilted smectic phases, in which the molecules are confined to layers, sorting out layer-by-layer sequences of azimuthal orientations of tilted molecules [56,57]. In this context, the general theory of resonant scattering was applied to the smectic case [58]. This formalism has recently been applied in a comprehensive analysis of RSoXS scattering from the TB phase by Salamończyk et al. [59,60], which supports the duplex helical model.

RSoXS at the carbon K-edge (incident wavelength, $\lambda = 4.4$ nm) gives a range of scattering vectors $q < 2\pi/2.2$ nm, probing length scales through the nanometer range down to ~ 2 nm: molecular, but not atomic, size. In this q range, molecular subcomponents such as the biphenyls in CB7CB act nearly as composite entities in the scattering process, being describable by second-rank molecular polarizability tensor scattering cross-sections, as in deGennes' formulation of light scattering by fluctuations in director orientation [36]. In analogy with visible light microscopy, RSoXS could even be used to visualize patterns of birefringence of LC phases and textures with X-ray resolution using depolarized transmission.

In probing the DHTC model of the TB phase, we first consider the RSoXS from individual filaments, illustrated in Supplementary Figure S16, focusing on the essential qualitative features of the scattering in the simplest geometry. This figure shows about 1.5 pitches

of the $\psi = 0$ DHT chain in Figure 5b, represented by space-filling models of CB7CB. In a typical experiment, the sample cell with the LC between silicon nitride windows is oriented parallel to the Figure plane, the TB helix axes of the LC are aligned parallel to the windows, and we consider illuminating a domain with the local helix axis vertical, as shown in the figure. Incident X-rays pass through the image plane and are forward-scattered onto a 2D detector behind. The incident and scattered directions can be chosen so that the scattering vector q is parallel to the DHTC z-axis. In this example, we take the incident X-ray polarization, i , to be horizontal. The helical winding of the filament is apparent in the figure, with the director giving the orientation of a principal axis of the polarizability tensor following a helical trajectory, as shown in Figures 1 and 4. According to deGennes, the depolarized scattering field amplitude probing director orientation is approximately

$$E_d(z) \propto (f \cdot z)(\delta n(z) \cdot i), \quad (25)$$

where f is the outgoing polarization, nearly parallel to z , and $\delta n(z)$ is the angular deviation from z . The key feature of this relation is that E is linear in $\delta n(z)$, so that the sinusoidal projection of the helix structure onto the i - z plane gives a sinusoidally varying scattering amplitude as $\delta n(z) = \sin(q_H z)$, which, in turn, produces scattering at $q = q_H$. This is the basis of the claim that the depolarized scattering peak determines the helix pitch $p_H = 2\pi/q_H$, which clearly should be applicable to scattering from a single DHTC. In addition to the helical undulation, the DHTC exhibits smaller-scale roughness, a result of the precessing biaxiality discussed in the previous section. Inspection of the DHCT shows that, like in Figure 4b, there are, in general, four distinct projections of the biaxial order on any vertical plane. Scattering from these variations has amplitude

$$E_p(z) \propto (p(z) \cdot i)(p(z) \cdot i), \quad (26)$$

where $p(z)$ is the biaxial orientation vector. Here, the scattered amplitude is independent of the sign of $p(z)$ so that the projection of $p(z)$ onto a vertical plane $\delta n(z) = \sin(q_H z)$ generates a polarized scattering amplitude $E_p(z) \propto \cos(2q_H z)$, the second harmonic of the scattering from the helix, explicitly showing that the periodicity of the biaxiality is a half-pitch: flipping the rectangles around $\Delta\varphi = \pi$ does not change their biaxial polarizability. All the DHT chains presented here share this property. Salamończyk et al. have pointed out that in the scattering from columns of helical precessing tilted rods, averaging together pairs of columns shifted relatively in phase by a half-period of their biaxial polarizability renders the net polarizability the same in every quarter period and the second harmonic disappears. In the few experiments where the second harmonic might have been seen, it has not been observed [30,31,59], indicating that such averaging may be taking place in the TB phase. In the case of the DHTCs, shifting a pair of chains by two segments and averaging will eliminate the second harmonic. However, achieving this in arrays of DHTCs may be problematic since frustration effects come into play on the closest-packed 2D hexagonal lattices.

2.9. Asymmetric Elasticity of the Twist-Bend Helix

A relevant feature of the lamellar-like helical ordering of the TB phase is the unexpected asymmetry in the response of the TB helix pitch to compressive or dilative stress [30]. In typical fluid lamellar liquid crystals, such as the smectics A and C, stresses tending to change the layer thickness encountered in typical textures, for example, in planar-aligned cells or in focal conic powders in capillaries, exhibit little observable variation in layer spacing in X-ray scattering experiments, except near phase transitions where the compressional elastic constant can become small. In the TBX regime of CB7CB, the layer spacing increases with increasing temperature, putting the layer system under compressive stress upon heating, producing a well-defined minimum trajectory vs. increasing temperature, making RSOXS with slow heating the preferred method for determining TB helix pitch. The layer spacing can be significantly increased in an irregular fashion from this minimum

value by dilative stresses appearing upon cooling. The DHT chaining thus responds in an asymmetric way to stress along z , with the end-to-end packing of the molecules in the chains resisting compression but the steric association of the overall structure being rather soft against stretching. Such effects cause a rather wide variation in the layer spacing measured by freeze-fracture, as discussed above and in the Supplementary Materials (Figures S17–S19).

2.10. Model Systems of Bent, Rigid Molecules

We sought to explore the role of molecular bend in other TB systems. The only others of which we are aware and for which data sets of p_H vs. θ_H are available are the mean-field theoretical model for bent rods of Greco et al. [61] and the Monte Carlo simulation of Greco et al. of hard spheres assembled to make steric circular arcs [62]. These models are of particular interest because they treat collective TB behavior for bent objects that are rigid. Figure 7a and b show plots of B_H vs. $\sin\theta_H$ calculated from $p_H(\theta_H)$ for the arcs and bent rods, respectively. The black line in each plot is drawn through the origin and $B_H(\theta_H)$ for the smallest θ_H . The general behavior of $B_H(\sin\theta_H)$ is similar to that of the CB7CB mixtures in Figure 3a, but with a tendency to increase relative to the black line with increasing $\sin\theta_H$, which is also seen weakly in neat CB7CB (Figure 3a).

In the case of the hard, circular arcs, we carried out the R_{mol} construction of Figure 3b, with the result shown in Figure 7a, finding $R_{mol} = 12.6$ in units of the sphere diameter, σ . The corresponding $B_{mol} = 1/R_{mol} = 0.08/\sigma$ is comparable to the $B = 0.1/\sigma$ extrapolation of the black line, indicating a relation between the PB and TBX limits similar to that in the CB7CB mixtures. This makes the hard arcs a very interesting system for exploration of the DHTC structure.

Turning to the bent rod case, Figure 7b shows that $B_H(\theta_H)$ obeys $B_H = S \sin q_H$ rather well for $\theta_H < 15^\circ$, with a slope $S = 0.56/L$, where L is the length of one of the arms in the bent rods. In Figure 7b, we have used the small-angle value of S to extrapolate to $\theta_H = 90^\circ$ in order to determine the radius of the cylinder $R = 1/S$ in the PB regime. The resulting construction using the shape of the simulated bent rods shows a quite reasonable PB limit. This is an exciting result because this model approaches understanding the TBX regime from a mean-field statistical mechanical approach that is entirely different from the geometrical model building that we have employed here. That it captures the essence of the geometry of “the line” offers an opportunity to understand in detail the evolution of the local geometry to keep the system on “the line” in the absence of changes in molecular conformation.

Both models consider rigid molecules and yet seem to exhibit the same essential geometrical behavior as the CB7CB system, which was rationalized based on nanophase segregation of flexible (the central alkyl linker and the tail ends) and rigid molecular subcomponents (cores): the molecular ends find entropic freedom by associating with the flexible cores. We propose that in systems of rigid, bent, hard particles, the analogous association is between the particle ends and the free volume available in the pockets of difficult-to-fill space created by molecular bend.

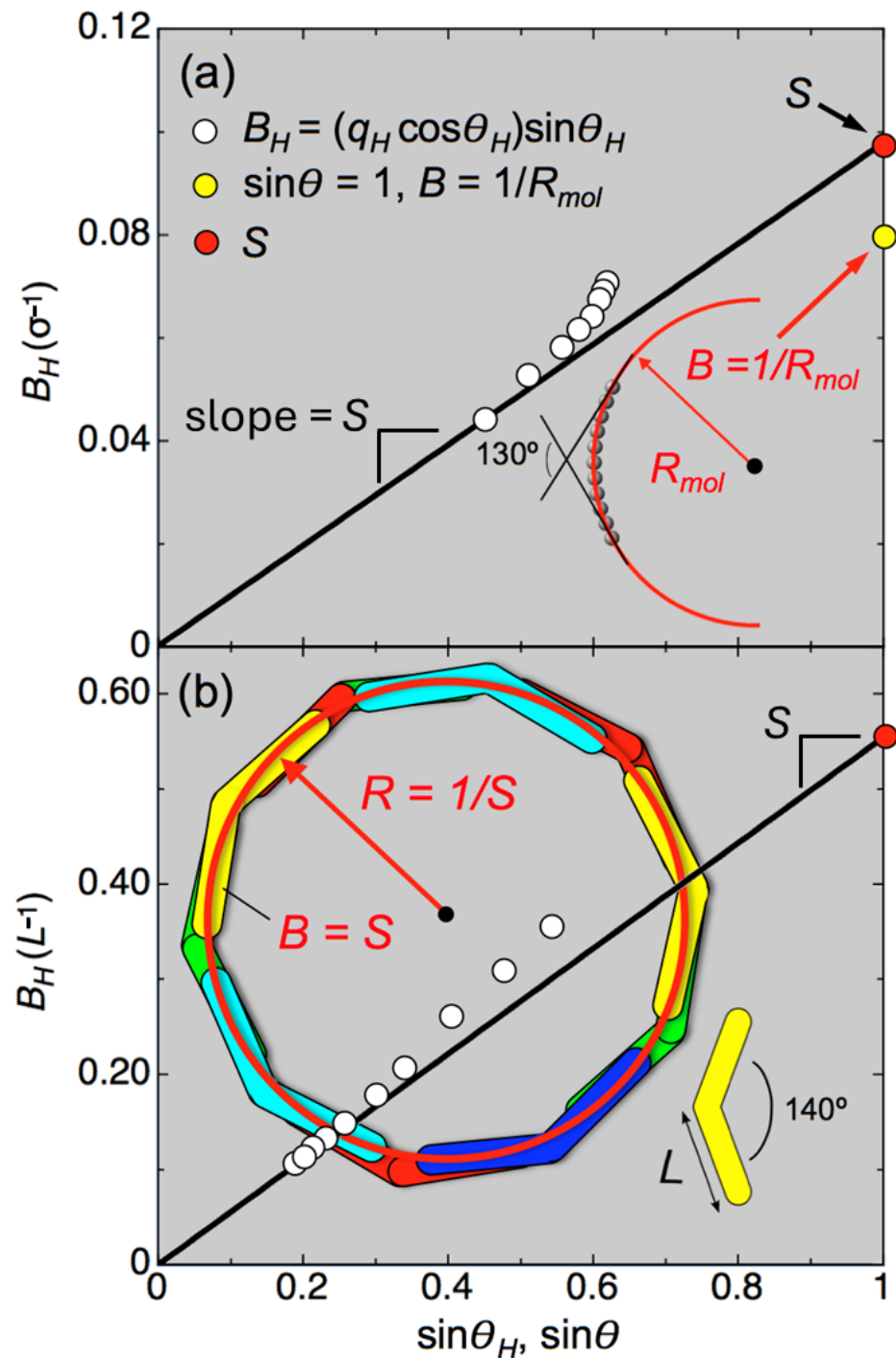


Figure 7. $B(\theta_H)$ vs. $\sin \theta_H$, analogous to those of Figure 3a, obtained in various ways for two statistical mechanical model systems of interacting bent particles. The black lines are drawn to match the measured bend at the smallest θ_H . (a) Monte Carlo simulation of TB ordering of steric particles made by rigidly chaining 11 hard spheres in the form of circular arcs [61]. The length scale is the sphere diameter, σ . The molecular curvature construction of Figure 3b is also sketched, giving a molecular bend $B_m = 1/R_{mol} = (2\pi \cdot 50)/(360 \cdot 11) = 0.079/\sigma$, plotted as the yellow dot at $\theta = 90^\circ$. B_m is comparable to the slope of the line, as was found for CB7CB in Figure 3. (b) Generalized Maier-Saupe mean-field theory of the TB ordering of bent rods in which the rod halves were considered as independent interaction centers [62]. Also sketched is the PB construction of Figure 3c, where R is simply set to $R = 1/S$, i.e., the bend B in the circular construction is set to S , and the bend on “the line” extrapolated to $\theta = 90^\circ$. It seems remarkable that a mean-field model can capture this geometry.

3. Conclusions

The principal outcome of this work has been to demonstrate experimentally and interpret structurally a remarkable internal constraint on the heliconical structure of the twist-bend phase formed by the bent molecular dimer CB7CB and its mixtures. This geometrical invariance equates the magnitude of director bend at a large cone angle (low temperature in the TB phase) to the magnitude of biaxial twist at a small cone angle (high temperature in the TB phase), relating both to the mean molecular curvature of the CB7CB molecule. The bend of the CB7CB molecules enables them to self-assemble into spontaneously helical duplex chains in which there is a fixed contour length along the chain for a single pitch, roughly half the molecular length, established by brickwork-like packing of molecules along each chain. This structuring introduces natural nanoscale length, producing the above constraint in a way that is not readily apparent from director elasticity or its symmetry-allowed modifications.

This, and the X-ray observation of half-molecular length periodicity along the TB helix, leads to the model of the self-assembly of half-molecule-long segments into duplex helical tiled chains of molecules as the basic structural element of the TB phase presented here. The geometrical constraint then shows up as $\Delta\varphi = 45^\circ$ director bend jumps from segment to segment in the PB ring limit and 45° biaxial twist jumps in the TBX limit. As noted in the text, there is no symmetry requirement for this equality. The structural organization of the DHT chains should accommodate a range of possible $\Delta\varphi$'s per segment. For example, it appears that DTC5C7/DTSe [31] and AZO7 [63], with ratios of $p_H/p_m \sim 6$ in the TBX regime, have a $\Delta\varphi \sim 60^\circ/\text{jump}$, and there seems to be no structural impediment to 90° per jump [48]. Since these $\Delta\varphi \sim 60^\circ$ materials are unlikely to have comparably large bend jumps in the PB regime, they will not move on “the line”. Thus, how general the CB7CB behavior is among the TB materials remains to be seen. However, in any case, the CB7CB scenario appears to offer a useful benchmark for relating the molecular structure and macroscopic behavior in TB phases. If the data are not “on the line” as for the simulated systems in Figure 7, the deviations can be explored by comparison with CB7CB ideal elastic behavior. For systems exhibiting the CB7CB scenario, there remains the question of relating the slope S of the B_H vs. $\sin\theta_H$ curve to the molecular shape. CB7CB also turns out to be extremely simple in this regard (maybe not just a coincidence). In the case of CB7CB, the extended molecule is almost circular, so the B_{mol} is readily determined from the molecular shape and S matches this bend very well. In general, however, it will not be so easy to assess molecular bend. For example, flexibility in molecules with longer aliphatic linkers will likely make B_{mol} smaller than estimates based on extended molecular shape. This leads to the question of how to design calculational or simulation schemes of the pure bend regime that can quantitatively predict the TB structure by determining B_{mol} to get S .

In closing, this exploration of CB7CB mixtures sheds light on the intricate interplay between concentration, temperature, and geometrical constraints in heliconical structures. While this study describes longitudinal molecular connections and self-assembly phenomena in stabilizing such structures, questions regarding the generalizability of these findings to other compounds persist. Further investigation into the molecular behavior across different regimes, as well as the development of computational and simulation methodologies, promises to advance our understanding of helical structures and empower the design of novel functional materials.

4. Materials and Methods

CB7CB (4',4'-(heptane-1,7-diyl)bis([(1',1''-biphenyl]-4''-carbonitrile))) was synthesized by two different methods as described previously [30]. 5CB (4-cyano-4'-pentylbiphenyl) was purchased from Sigma-Aldrich and used as received. Polarized transmission optical microscopy was carried out in Instec 3.2 μm unidirectionally rubbed commercial cells and home-made untreated cells. The birefringence of CB7CB and its mixtures with 5CB was measured in the PLM with a Zeiss Ehringhaus Rotary Compensator. We performed resonant X-ray scattering experiments at beamline 11.0.1.2 at the Advanced Light Source, Lawrence

Berkeley National Laboratory. The samples for FFTEM experiments were prepared by sandwiching the LC mixtures between 2 mm by 3 mm untreated glass slides spaced by a several-micron-thick gap and observing the cell on a hot stage under a PLM, as previously described [9,10]. Detailed experimental methods and materials are included in the Supplementary Materials.

Supplementary Materials: The following supporting information can be downloaded at <https://www.mdpi.com/article/10.3390/cryst14070583/s1>: Materials and Methods, Figures S1–S19, Table S1, and References [43,52,64–76].

Author Contributions: Conceptualization, N.A.C.; Methodology, M.S., C.Z., L.R., D.B., D.M.W., J.E.M., M.A.G., and N.A.C.; Formal analysis, M.R.T., M.S., and K.A.G.; Investigation, M.R.T., M.S., D.C., L.R., A.K., J.Y., J.B.H., X.W., D.B., and N.A.C.; Resources, L.F., A.S., J.H.P., M.M., and E.K.; Data curation, M.R.T., M.S., K.A.G., D.C., C.Z., J.B.H., X.W., C.W., and A.H.; Writing—original draft, M.R.T., M.S., L.R., and N.A.C.; Writing—review and editing, M.S., J.E.M., and N.A.C.; Supervision, J.E.M., M.A.G., and N.A.C.; Project administration, N.A.C.; Funding acquisition, N.A.C. and L.R. All authors have read and agreed to the published version of the manuscript.

Funding: This work was supported by NSF MRSEC Grant DMR-1420736, by the Institute for Complex and Adaptive Matter Postdoctoral Fellowship Award OCG5711B, and by ED GAANN Award P200A120014. LR acknowledges support from NSF grant DMR-1001240 and from the Simons Investigator award from the Simons Foundation. We acknowledge the use of beamline 11.0.1.2 of the Advanced Light Source at Lawrence Berkeley National Laboratory supported by the Director of the Office of Science, Office of Basic Energy Sciences, of the U.S. Department of Energy under contract no. DE-AC02-05CH11231.

Data Availability Statement: The original data presented in the study are openly available at <https://osf.io/pghcw/>, and are included in the article/Supplementary Materials, further inquiries can be directed to the corresponding author.

Conflicts of Interest: The authors declare no competing financial interests.

References

1. Link, D.R.; Natale, G.; Shao, R.; Maclennan, J.E.; Clark, N.A.; Körblova, E.; Walba, D.M. Spontaneous Formation of Macroscopic Chiral Domains in a Fluid Smectic Phase of Achiral Molecules. *Science* **1997**, *278*, 1924–1927. [[CrossRef](#)]
2. Sekine, T.; Niori, T.; Sone, M.; Watanabe, J.; Choi, S.-W.; Takanishi, Y.; Takezoe, H. Origin of Helix in Achiral Banana-Shaped Molecular Systems. *Jpn. J. Appl. Phys.* **1997**, *36*, 6455–6463. [[CrossRef](#)]
3. Takezoe, H.; Takanishi, Y. Bent-Core Liquid Crystals: Their Mysterious and Attractive World. *Jpn. J. Appl. Phys.* **2006**, *45*, 597. [[CrossRef](#)]
4. Reddy, R.A.; Tschierske, C. Bent-Core Liquid Crystals: Polar Order, Superstructural Chirality and Spontaneous Desymmetrisation in Soft Matter Systems. *J. Mater. Chem.* **2006**, *16*, 907–961. [[CrossRef](#)]
5. Dressel, C.; Weissflog, W.; Tschierske, C. Spontaneous Mirror Symmetry Breaking in a Re-Entrant Isotropic Liquid. *Chem. Commun.* **2015**, *51*, 15850–15853. [[CrossRef](#)]
6. Dressel, C.; Liu, F.; Prehm, M.; Zeng, X.; Ungar, G.; Tschierske, C. Dynamic Mirror-Symmetry Breaking in Bicontinuous Cubic Phases. *Angew. Chem. Int. Ed.* **2014**, *53*, 13115–13120. [[CrossRef](#)]
7. Coleman, D.A.; Fernsler, J.; Chattham, N.; Nakata, M.; Takanishi, Y.; Körblova, E.; Link, D.R.; Shao, R.-F.; Jang, W.G.; Maclennan, J.E.; et al. Polarization-Modulated Smectic Liquid Crystal Phases. *Science* **2003**, *301*, 1204–1211. [[CrossRef](#)]
8. Porada, J.H.; Blunk, D. Phasmidic Indigoid Liquid Crystals. *J. Mater. Chem.* **2010**, *20*, 2956–2958. [[CrossRef](#)]
9. Hough, L.E.; Jung, H.T.; Krüerke, D.; Heberling, M.S.; Nakata, M.; Jones, C.D.; Chen, D.; Link, D.R.; Zasadzinski, J.; Heppke, G.; et al. Helical Nanofilament Phases. *Science* **2009**, *325*, 456–460. [[CrossRef](#)] [[PubMed](#)]
10. Hough, L.E.; Spannuth, M.; Nakata, M.; Coleman, D.A.; Jones, C.D.; Dantlgraber, G.; Tschierske, C.; Watanabe, J.; Körblova, E.; Walba, D.M.; et al. Chiral Isotropic Liquids from Achiral Molecules. *Science* **2009**, *325*, 452–456. [[CrossRef](#)] [[PubMed](#)]
11. Meyer, R.B. Structural Problems in Liquid Crystal Physics. Les Houches Summer School in Theoretical Physics, 1973. In *Molecular Fluids*; Balian, R., Weil, G., Eds.; Gordon and Breach: New York, NY, USA, 1976; pp. 273–373.
12. Dozov, I. On the Spontaneous Symmetry Breaking in the Mesophases of Achiral Banana-Shaped Molecules. *Europhys. Lett.* **2001**, *56*, 247. [[CrossRef](#)]
13. Memmer, R. Liquid Crystal Phases of Achiral Banana-Shaped Molecules: A Computer Simulation Study. *Liq. Cryst.* **2002**, *29*, 483–496. [[CrossRef](#)]

14. Panov, V.P.; Nagaraj, M.; Vij, J.K.; Panarin, Y.P.; Kohlmeier, A.; Tamba, M.G.; Lewis, R.A.; Mehl, G.H. Spontaneous Periodic Deformations in Nonchiral Planar-Aligned Bimesogens with a Nematic-Nematic Transition and a Negative Elastic Constant. *Phys. Rev. Lett.* **2010**, *105*, 167801. [[CrossRef](#)]
15. Cestari, M.; Diez-Berart, S.; Dunmur, D.A.; Ferrarini, A.; de la Fuente, M.R.; Jackson, D.J.B.; Lopez, D.O.; Luckhurst, G.R.; Perez-Jubindo, M.A.; Richardson, R.M.; et al. Phase Behavior and Properties of the Liquid-Crystal Dimer 1'',7''-Bis(4-Cyanobiphenyl-4'-Yl) Heptane: A Twist-Bend Nematic Liquid Crystal. *Phys. Rev. E* **2011**, *84*, 031704. [[CrossRef](#)]
16. Chen, D.; Nakata, M.; Shao, R.; Tuchband, M.R.; Shuai, M.; Baumeister, U.; Weissflog, W.; Walba, D.M.; Glaser, M.A.; Maclennan, J.E.; et al. Twist-Bend Heliconical Chiral Nematic Liquid Crystal Phase of an Achiral Rigid Bent-Core Mesogen. *Phys. Rev. E* **2014**, *89*, 022506. [[CrossRef](#)] [[PubMed](#)]
17. Wang, Y.; Singh, G.; Agra-Kooijman, D.M.; Gao, M.; Bisoyi, H.K.; Xue, C.; Fisch, M.R.; Kumar, S.; Li, Q. Room Temperature Heliconical Twist-Bend Nematic Liquid Crystal. *CrystEngComm* **2015**, *17*, 2778–2782. [[CrossRef](#)]
18. Tamba, M.G.; Baumeister, U.; Pelzl, G.; Weissflog, W. Banana-Calamitic Dimers: Unexpected Mesophase Behaviour by Variation of the Direction of Ester Linking Groups in the Bent-Core Unit. *Liq. Cryst.* **2010**, *37*, 853–874. [[CrossRef](#)]
19. Tripathi, C.S.P.; Losada-Pérez, P.; Glorieux, C.; Kohlmeier, A.; Tamba, M.-G.; Mehl, G.H.; Leys, J. Nematic-Nematic Phase Transition in the Liquid Crystal Dimer CBC9CB and Its Mixtures with 5CB: A High-Resolution Adiabatic Scanning Calorimetric Study. *Phys. Rev. E* **2011**, *84*, 041707. [[CrossRef](#)] [[PubMed](#)]
20. Mandle, R.J.; Voll, C.C.A.; Lewis, D.J.; Goodby, J.W. Etheric Bimesogens and the Twist-Bend Nematic Phase. *Liq. Cryst.* **2015**, *43*, 13–21. [[CrossRef](#)]
21. Gorecka, E.; Vaupotič, N.; Zep, A.; Pocięcha, D.; Yoshioka, J.; Yamamoto, J.; Takezoe, H. A Twist-Bend Nematic (NTB) Phase of Chiral Materials. *Angew. Chem.* **2015**, *127*, 10293–10297. [[CrossRef](#)]
22. Jansze, S.M.; Martínez-Felipe, A.; Storey, J.M.D.; Marcellis, A.T.M.; Imrie, C.T. A Twist-Bend Nematic Phase Driven by Hydrogen Bonding. *Angew. Chem. Int. Ed.* **2015**, *54*, 643–646. [[CrossRef](#)]
23. Adlem, K.; Čopič, M.; Luckhurst, G.R.; Mertelj, A.; Parri, O.; Richardson, R.M.; Snow, B.D.; Timimi, B.A.; Tuffin, R.P.; Wilkes, D. Chemically Induced Twist-Bend Nematic Liquid Crystals, Liquid Crystal Dimers, and Negative Elastic Constants. *Phys. Rev. E* **2013**, *88*, 022503. [[CrossRef](#)]
24. Henderson, P.A.; Imrie, C.T. Methylene-Linked Liquid Crystal Dimers and the Twist-Bend Nematic Phase. *Liq. Cryst.* **2011**, *38*, 1407–1414. [[CrossRef](#)]
25. Mandle, R.J.; Goodby, J.W. A Liquid Crystalline Oligomer Exhibiting Nematic and Twist-Bend Nematic Mesophases. *ChemPhysChem* **2016**, *17*, 967–970. [[CrossRef](#)]
26. Panov, V.; Song, J.-K.; Mehl, G.H.; Vij, J. The Beauty of Twist-Bend Nematic Phase: Fast Switching Domains, First Order Fréedericksz Transition and a Hierarchy of Structures. *Crystals* **2021**, *11*, 621. [[CrossRef](#)]
27. Nava, G.; Ciciulla, F.; Iadlovská, O.S.; Lavrentovich, O.D.; Simoni, F.; Lucchetti, L. Pitch Tuning Induced by Optical Torque in Heliconical Cholesteric Liquid Crystals. *Phys. Rev. Res.* **2019**, *1*, 033215. [[CrossRef](#)]
28. Nava, G.; Ciciulla, F.; Simoni, F.; Iadlovská, O.; Lavrentovich, O.D.; Lucchetti, L. Heliconical Cholesteric Liquid Crystals as Electrically Tunable Optical Filters in Notch and Bandpass Configurations. *Liq. Cryst.* **2021**, *48*, 1534–1543. [[CrossRef](#)]
29. Chen, D.; Porada, J.H.; Hooper, J.B.; Klitnick, A.; Shen, Y.; Tuchband, M.R.; Korblóva, E.; Bedrov, D.; Walba, D.M.; Glaser, M.A.; et al. Chiral Heliconical Ground State of Nanoscale Pitch in a Nematic Liquid Crystal of Achiral Molecular Dimers. *Proc. Natl. Acad. Sci. USA* **2013**, *110*, 15931–15936. [[CrossRef](#)]
30. Zhu, C.; Tuchband, M.R.; Young, A.; Shuai, M.; Scarbrough, A.; Walba, D.M.; Maclennan, J.E.; Wang, C.; Hexemer, A.; Clark, N.A. Resonant Carbon K-Edge Soft X-ray Scattering from Lattice-Free Heliconical Molecular Ordering: Soft Dilative Elasticity of the Twist-Bend Liquid Crystal Phase. *Phys. Rev. Lett.* **2016**, *116*, 147803. [[CrossRef](#)]
31. Stevenson, W.D.; Ahmed, Z.; Zeng, X.B.; Welch, C.; Ungar, G.; Mehl, G.H. Molecular Organization in the Twist-Bend Nematic Phase by Resonant X-ray Scattering at the Se K-Edge and by SAXS, WAXS and GIXRD. *Phys. Chem. Chem. Phys.* **2016**, *19*, 13449–13454. [[CrossRef](#)]
32. Dozov, I.; Luckhurst, G.R. Setting Things Straight in 'The Twist-Bend Nematic: A Case of Mistaken Identity'. *Liq. Cryst.* **2020**, *47*, 2098–2115. [[CrossRef](#)]
33. Samulski, E.T. The Ever Elusive, Yet-to-Be-Discovered Twist-Bend Nematic Phase. *Crystals* **2023**, *13*, 1648. [[CrossRef](#)]
34. Samulski, E.T.; Vanakaras, A.G.; Photinos, D.J. The Twist Bend Nematic: A Case of Mistaken Identity. *Liq. Cryst.* **2020**, *47*, 2092–2097. [[CrossRef](#)]
35. Samulski, E.T.; Reyes-Arango, D.; Vanakaras, A.G.; Photinos, D.J. All Structures Great and Small: Nanoscale Modulations in Nematic Liquid Crystals. *Nanomaterials* **2022**, *12*, 93. [[CrossRef](#)]
36. De Gennes, P.G.; Prost, J. *The Physics of Liquid Crystals*; Clarendon Press: Oxford, UK, 1995; ISBN 978-0-19-851785-6.
37. Borshch, V.; Kim, Y.-K.; Xiang, J.; Gao, M.; Jákli, A.; Panov, V.P.; Vij, J.K.; Imrie, C.T.; Tamba, M.G.; Mehl, G.H.; et al. Nematic Twist-Bend Phase with Nanoscale Modulation of Molecular Orientation. *Nat. Commun.* **2013**, *4*, 2635. [[CrossRef](#)]
38. Tuchband, M.R.; Shuai, M.; Graber, K.A.; Chen, D.; Zhu, C.; Radzihovskiy, L.; Klitnick, A.; Foley, L.M.; Scarbrough, A.; Porada, J.H.; et al. Double-Helical Tiled Chain Structure of the Twist-Bend Liquid Crystal Phase in CB7CB. *arXiv* **2017**, arXiv:1703.10787. [[CrossRef](#)]
39. Jákli, A.; Lavrentovich, O.D.; Selinger, J.V. Physics of Liquid Crystals of Bent-Shaped Molecules. *Rev. Mod. Phys.* **2018**, *90*, 045004. [[CrossRef](#)]

40. Barry, E.; Hensel, Z.; Dogic, Z.; Shribak, M.; Oldenbourg, R. Entropy-Driven Formation of a Chiral Liquid-Crystalline Phase of Helical Filaments. *Phys. Rev. Lett.* **2006**, *96*, 967–970. [[CrossRef](#)]
41. Kolli, H.B.; Cinacchi, G.; Ferrarini, A.; Giacometti, A. Chiral Self-Assembly of Helical Particles. *Faraday Discuss.* **2016**, *186*, 171–186. [[CrossRef](#)]
42. Clark, N.A.; Meyer, R.B. Strain-induced Instability of Monodomain Smectic A and Cholesteric Liquid Crystals. *Appl. Phys. Lett.* **1973**, *22*, 493–494. [[CrossRef](#)]
43. Challa, P.K.; Borshch, V.; Parri, O.; Imrie, C.T.; Sprunt, S.N.; Gleeson, J.T.; Lavrentovich, O.D.; Jáklí, A. Twist-Bend Nematic Liquid Crystals in High Magnetic Fields. *Phys. Rev. E* **2014**, *89*, 060501. [[CrossRef](#)]
44. Parthasarathi, S.; Rao, D.S.S.; Palakurthy, N.B.; Yelamagad, C.V.; Krishna Prasad, S. Binary System Exhibiting the Nematic to Twist-Bend Nematic Transition: Behavior of Permittivity and Elastic Constants. *J. Phys. Chem. B* **2016**, *120*, 5056–5062. [[CrossRef](#)] [[PubMed](#)]
45. Meyer, C.; Luckhurst, G.R.; Dozov, I. The Temperature Dependence of the Heliconical Tilt Angle in the Twist-Bend Nematic Phase of the Odd Dimer CB7CB. *J. Mater. Chem. C* **2015**, *3*, 318–328. [[CrossRef](#)]
46. Jokisaari, J.P.; Luckhurst, G.R.; Timimi, B.A.; Zhu, J.; Zimmermann, H. Twist-Bend Nematic Phase of the Liquid Crystal Dimer CB7CB: Orientational Order and Conical Angle Determined by ¹²⁹Xe and ²H NMR Spectroscopy. *Liq. Cryst.* **2015**, *42*, 708–721. [[CrossRef](#)]
47. Vaupotič, N.; Curk, S.; Osipov, M.A.; Čepič, M.; Takezoe, H.; Gorecka, E. Short-Range Smectic Fluctuations and the Flexoelectric Model of Modulated Nematic Liquid Crystals. *Phys. Rev. E* **2016**, *93*, 022704. [[CrossRef](#)]
48. Hori, K.; Iimuro, M.; Nakao, A.; Toriumi, H. Conformational Diversity of Symmetric Dimer Mesogens, α,ω -Bis(4,4'-Cyanobiphenyl)Octane, -Nonane, α,ω -Bis(4-Cyanobiphenyl-4'-Yloxy-carbonyl)Propane, and -Hexane in Crystal Structures. *J. Mol. Struct.* **2004**, *699*, 23–29. [[CrossRef](#)]
49. McBride, C.; Vega, C. A Monte Carlo Study of the Influence of Molecular Flexibility on the Phase Diagram of a Fused Hard Sphere Model. *J. Chem. Phys.* **2002**, *117*, 10370–10379. [[CrossRef](#)]
50. Tamba, M.G.; Salili, S.M.; Zhang, C.; Jáklí, A.; Mehl, G.H.; Stannarius, R.; Eremin, A. A Fibre Forming Smectic Twist-Bend Liquid Crystalline Phase. *RSC Adv.* **2015**, *5*, 11207–11211. [[CrossRef](#)]
51. Mandle, R.J.; Archbold, C.T.; Sarju, J.P.; Andrews, J.L.; Goodby, J.W. The Dependency of Nematic and Twist-Bend Mesophase Formation on Bend Angle. *Sci. Rep.* **2016**, *6*, 36682. [[CrossRef](#)]
52. Spal, R.; Chen, C.-E.; Egami, T.; Nigrey, P.J.; Heeger, A.J. X-ray Scattering Study of One-Dimensional Lattice Dynamics in Hg 3- δ As F 6. *Phys. Rev. B* **1980**, *21*, 3110. [[CrossRef](#)]
53. Axe, J.D. Fluctuations and Freezing in a One-Dimensional Liquid: Hg3- δ AsF6. In *Solitons and Condensed Matter Physics*; Springer: Berlin/Heidelberg, Germany, 1978; pp. 234–245.
54. Zhu, C.; Wang, C.; Young, A.; Liu, F.; Gunkel, I.; Chen, D.; Walba, D.; Maclennan, J.; Clark, N.; Hexemer, A. Probing and Controlling Liquid Crystal Helical Nanofilaments. *Nano Lett.* **2015**, *15*, 3420–3424. [[CrossRef](#)]
55. Bates, M.; Frenkel, D. Influence of Polydispersity on the Phase Behavior of Colloidal Liquid Crystals: A Monte Carlo Simulation Study. *J. Chem. Phys.* **1998**, *109*, 6193–6199. [[CrossRef](#)]
56. Mach, P.; Pindak, R.; Levelut, A.-M.; Barois, P.; Nguyen, H.T.; Huang, C.C.; Furenid, L. Structural Characterization of Various Chiral Smectic-C Phases by Resonant X-ray Scattering. *Phys. Rev. Lett.* **1998**, *81*, 1015–1018. [[CrossRef](#)]
57. Mach, P.; Pindak, R.; Levelut, A.-M.; Barois, P.; Nguyen, H.T.; Baltes, H.; Hird, M.; Toyne, K.; Seed, A.; Goodby, J.W.; et al. Structures of Chiral Smectic-C Mesophases Revealed by Polarization-Analyzed Resonant X-ray Scattering. *Phys. Rev. E* **1999**, *60*, 6793–6802. [[CrossRef](#)] [[PubMed](#)]
58. Levelut, A.-M.; Pansu, B. Tensorial X-ray Structure Factor in Smectic Liquid Crystals. *Phys. Rev. E* **1999**, *60*, 6803. [[CrossRef](#)] [[PubMed](#)]
59. Salamończyk, M.; Vaupotič, N.; Pocięcha, D.; Wang, C.; Zhu, C.; Gorecka, E. Structure of Nanoscale-Pitch Helical Phases: Blue Phase and Twist-Bend Nematic Phase Resolved by Resonant Soft X-ray Scattering. *Soft Matter* **2017**, *13*, 6694–6699. [[CrossRef](#)]
60. Salamończyk, M.; Mandle, R.J.; Makal, A.; Liebman-Peláez, A.; Feng, J.; Goodby, J.W.; Zhu, C. Double Helical Structure of the Twist-Bend Nematic Phase Investigated by Resonant X-ray Scattering at the Carbon and Sulfur K-Edges. *Soft Matter* **2018**, *14*, 9760–9763. [[CrossRef](#)]
61. Greco, C.; Ferrarini, A. Entropy-Driven Chiral Order in a System of Achiral Bent Particles. *Phys. Rev. Lett.* **2015**, *115*, 147801. [[CrossRef](#)]
62. Greco, C.; Luckhurst, G.R.; Ferrarini, A. Molecular Geometry, Twist-Bend Nematic Phase and Unconventional Elasticity: A Generalised Maier-Saupe Theory. *Soft Matter* **2014**, *10*, 9318–9323. [[CrossRef](#)] [[PubMed](#)]
63. Zep, A.; Aya, S.; Aihara, K.; Ema, K.; Pocięcha, D.; Madrak, K.; Bernatowicz, P.; Takezoe, H.; Gorecka, E. Multiple Nematic Phases Observed in Chiral Mesogenic Dimers. *J. Mater. Chem. C* **2013**, *1*, 46–49. [[CrossRef](#)]
64. Ilavsky, J. Nika: Software for Two-Dimensional Data Reduction. *J. Appl. Crystallogr.* **2012**, *45*, 324–328. [[CrossRef](#)]
65. Zhang, F.; Ilavsky, J.; Long, G.G.; Quintana, J.P.G.; Allen, A.J.; Jemian, P.R. Glassy Carbon as an Absolute Intensity Calibration Standard for Small-Angle Scattering. *Metall. Mater. Trans. A* **2010**, *41*, 1151–1158. [[CrossRef](#)]
66. Salili, S.M.; Kim, C.; Sprunt, S.; Gleeson, J.T.; Parri, O.; Jáklí, A. Flow Properties of a Twist-Bend Nematic Liquid Crystal. *RSC Adv* **2014**, *4*, 57419–57423. [[CrossRef](#)]
67. Haller, I. Thermodynamic and Static Properties of Liquid Crystals. *Prog. Solid State Chem.* **1975**, *10*, 103–118. [[CrossRef](#)]

68. Li, J.; Wu, S.-T. Self-Consistency of Vuks Equations for Liquid-Crystal Refractive Indices. *J. Appl. Phys.* **2004**, *96*, 6253–6258. [[CrossRef](#)]
69. Mandle, R.J.; Goodby, J.W. A Twist-Bend Nematic to an Intercalated, Anticlinic, Biaxial Phase Transition in Liquid Crystal Bimesogens. *Soft Matter* **2016**, *12*, 1436–1443. [[CrossRef](#)] [[PubMed](#)]
70. Panov, V.P.; Vij, J.K.; Mehl, G.H. Twist-Bend Nematic Phase in Cyanobiphenyls and Difluoroterphenyls Bimesogens. *Liq. Cryst.* **2016**, 1–13.
71. Gorecka, E.; Salamonczyk, M.; Zep, A.; Pocięcha, D.; Welch, C.; Ahmed, Z.; Mehl, G.H. Do the Short Helices Exist in the Nematic TB Phase? *Liq. Cryst.* **2015**, *42*, 1–7. [[CrossRef](#)]
72. Archbold, C.T.; Davis, E.J.; Mandle, R.J.; Cowling, S.J.; Goodby, J.W. Chiral Dopants and the Twist-Bend Nematic Phase—Induction of Novel Mesomorphic Behaviour in an Apolar Bimesogen. *Soft Matter* **2015**, *11*, 7547–7557. [[CrossRef](#)]
73. Gao, M.; Kim, Y.-K.; Zhang, C.; Borshch, V.; Zhou, S.; Park, H.-S.; Jáklí, A.; Lavrentovich, O.D.; Tamba, M.-G.; Kohlmeier, A.; et al. Direct Observation of Liquid Crystals Using Cryo-TEM: Specimen Preparation and Low-Dose Imaging: TEM of Liquid Crystals. *Microsc. Res. Tech.* **2014**, *77*, 754–772. [[CrossRef](#)]
74. Decressain, R.; Cochin, E.; Mansare, T.; More, M. Polymorphism and Dynamics of MBBA as Studied by NMR. *Liq. Cryst.* **1998**, *25*, 517–523. [[CrossRef](#)]
75. Mansaré, T.; Decressain, R.; Gors, C.; Dolganov, V.K. Phase Transformations and Dynamics Of 4-Cyano-4'-Pentylbiphenyl (5cb) By Nuclear Magnetic Resonance, Analysis Differential Scanning Calorimetry, And Wideangle X-ray Diffraction Analysis. *Mol. Cryst. Liq. Cryst.* **2002**, *382*, 97–111. [[CrossRef](#)]
76. Costello, M.J.; Fetter, R.; Höchli, M. Simple Procedures for Evaluating the Cryofixation of Biological Samples. *J. Microsc.* **1982**, *125*, 125–136. [[CrossRef](#)]

Disclaimer/Publisher's Note: The statements, opinions and data contained in all publications are solely those of the individual author(s) and contributor(s) and not of MDPI and/or the editor(s). MDPI and/or the editor(s) disclaim responsibility for any injury to people or property resulting from any ideas, methods, instructions or products referred to in the content.